

Argon offline-AMS source apportionment of organic aerosol over yearly cycles for an urban, rural and marine site in Northern Europe

C. Bozzetti¹, Y. Sosedova¹, M. Xiao¹, K. R. Daellenbach¹, V. Ulevicius², V. Dudoitis², G. Mordas², S. Byčenkienė², K. Plauškaitė², A. Vlachou¹, B. Golly³, B. Chazeau¹, J.-L. Besombes⁴, U. Baltensperger¹, J.-L. Jaffrezo³, J. G. Slowik¹, El Haddad¹, I., and A. S. H. Prévôt¹

[1] {Laboratory of Atmospheric Chemistry, Paul Scherrer Institute (PSI), 5232 Villigen-PSI, Switzerland}

[2] {Department of Environmental Research, SRI Center for Physical Sciences and Technology, LT-02300 Vilnius, Lithuania}

[3] {Université Grenoble Alpes, CNRS, LGGE, 38000 Grenoble, France}

[4] {Université Savoie Mont-Blanc, LCME, F-73000 Chambéry, France}

Correspondence to: A. S. H. Prévôt (andre.prevot@psi.ch); I. El Haddad (imad.el-haddad@psi.ch)

Abstract

The widespread use of Aerodyne aerosol mass spectrometers (AMS) has greatly improved real-time organic aerosol (OA) monitoring, providing mass spectra that contain sufficient information for source apportionment. However, AMS field deployments remain expensive and demanding, limiting the acquisition of long-term datasets at many sampling sites. The offline application of aerosol mass spectrometry entailing the analysis of nebulized water extracted filter samples (offline-AMS) increases the spatial coverage accessible to AMS measurements, being filters routinely collected at many stations worldwide.

PM₁ (particulate matter with an aerodynamic diameter <1 µm) filter samples were collected during an entire year in Lithuania at three different locations representative of three typical

environments of the South-East Baltic region: Vilnius (urban background), Rūgštelis (rural terrestrial), and Preila (rural coastal). Aqueous filter extracts were nebulized in Ar, yielding the first AMS measurements of water-soluble atmospheric organic aerosol (WSOA) without interference from air fragments. This enables direct measurement of the CO^+ fragment contribution, whose intensity is typically assumed to be equal to that of CO_2^+ . Offline-AMS spectra reveal that the water soluble $\text{CO}_2^+:\text{CO}^+$ ratio not only shows values systematically >1 but is also dependent on season, with lower values in winter than in summer.

AMS WSOA spectra were analyzed using positive matrix factorization (PMF), which yielded 4 factors. These factors included biomass burning OA (BBOA), local OA (LOA) contributing significantly only in Vilnius, and two oxygenated OA (OOA) factors, summer OOA (S-OOA) and background OOA (B-OOA) distinguished by their seasonal variability. The contribution of traffic exhaust OA (TEOA) was not resolved by PMF due to both low concentrations and low water solubility. Therefore, the TEOA concentration was estimated using a chemical mass balance approach, based on the concentrations of hopanes, specific markers of traffic emissions. AMS-PMF source apportionment results were consistent with those obtained from PMF applied to marker concentrations (i.e. major inorganic ions, OC/EC, and organic markers including polycyclic aromatic hydrocarbons and their derivatives, hopanes, long-chain alkanes, monosaccharides, anhydrous sugars, and lignin fragmentation products). OA was the largest fraction of PM_{10} and was dominated by BBOA during winter with an average concentration of $2 \mu\text{g m}^{-3}$ (53% of OA), while summer-OOA (S-OOA), probably related to biogenic emissions was the prevalent OA source during summer with an average concentration of $1.2 \mu\text{g m}^{-3}$ (45% of OA).

PMF ascribed a large part of the CO^+ explained variability (97%) to the OOA and BBOA factors. Accordingly we discuss a new CO^+ parameterization as a function of CO_2^+ , and $\text{C}_2\text{H}_4\text{O}_2^+$ fragments, which were selected to describe the variability of the OOA and BBOA factors.

1 Introduction

Atmospheric aerosols affect climate (Lohmann et al., 2004, Schwarze et al., 2006), human health (Dockery et al., 2005, Laden et al., 2000), and ecosystems on a global scale. Quantification and characterization of the main aerosol sources are crucial for the development of effective mitigation strategies. The Aerodyne aerosol mass spectrometer (AMS, Canagaratna et al., 2007) and aerosol chemical speciation monitor (ACSM, Ng et al.,

1 2011, Fröhlich et al., 2013) have greatly improved air quality monitoring by providing real-
2 time measurements of the non-refractory (NR) submicron aerosol (PM₁) components.
3 Analysis of organic mass spectra using positive matrix factorization (PMF, Paatero, 1997;
4 Paatero and Tapper, 1994) has enabled the quantitative separation of OA factors, which can
5 be subsequently related to major aerosol sources and formation processes (e.g. Lanz et al.,
6 2007; Lanz et al., 2010; Zhang et al., 2011; Ulbrich et al., 2009; Elser et al., 2016 a). Despite
7 its numerous advantages, AMS field deployment remains expensive and demanding, and
8 therefore most of the studies are typically restricted to short-time periods and a single (or few)
9 sampling site(s). The limited amount of long-term datasets suitable for OA source
10 apportionment severely limits model testing and validation (Aksoyoglu et al., 2011;
11 Aksoyoglu et al., 2014; Baklanov et al., 2014), as well as for the development of appropriate
12 pollution mitigation strategies. AMS analysis of aerosol filter samples (Lee et al., 2011; Sun
13 et al., 2011; Mihara and Mochida, 2011; Daellenbach et al., 2016), which are routinely
14 collected at many stations worldwide, broadens the temporal and spatial scales available for
15 AMS measurements.

16 In this study we present the application of the offline-AMS methodology described by
17 Daellenbach et al. (2016) to yearly cycles of filter samples collected in parallel at three
18 different locations in Lithuania between September 2013 and August 2014. The methodology
19 consists of water extraction of filter samples, followed by nebulization of the liquid extracts,
20 and subsequent measurement of the generated aerosol by high-resolution time-of-flight AMS
21 (HR-ToF AMS). In this work, organic aerosol water extracts were nebulized in Ar, permitting
22 direct measurement of the CO⁺ ion (Fig. S1), which is typically not directly quantified in
23 AMS data analysis due to interference with N₂⁺, but is instead estimated as being equal to
24 CO₂⁺ (Aiken et al., 2008). Direct measurement of CO₂⁺ better captures the variability in the
25 total OA mass and its elemental composition as well as potentially improving source
26 apportionment of ambient aerosol. Aerosol elemental ratios and oxidation state are of
27 particular relevance as they provide important constraints for understanding aerosol sources,
28 processes, and for the development of predictive aerosol models (Canagaratna et al., 2015).

29 Aerosol composition in the south-east Baltic region has so far received little attention. To our
30 knowledge the only investigation of OA sources in this area was during a five-day period of
31 intense land clearing activity occurring in the neighboring Russian enclave of Kaliningrad
32 (Ulevicius et al., 2016; Dudoitis et al., 2016), in which transported biomass burning emissions

dominated the aerosol loading. OA source contributions under less extreme conditions remain unstudied, with the most relevant measurements performed in Estonia with a mobile lab during March 2014 at two different locations (Elser et al., 2016b). On-road measurements revealed large traffic contributions with an increase of 20% from rural to urban environments. Also, residential biomass burning (BB) and oxygenated OA (OOA) contributions were found to be substantial.

In this study we present a complete source apportionment of the submicron OA fraction following the methodology described by Daellenbach et al. (2016) in order to quantify and characterize the main OA sources affecting the Lithuanian air quality. The three sampling stations were situated in the Vilnius suburb (urban background), Preila (rural coastal background), and Rūgšteliškis (rural terrestrial background), covering a wide geographical domain and providing a good overview of the most typical Lithuanian and south-eastern Baltic air quality conditions and environments. PMF analysis of offline-AMS measurements are compared with the results reported by Ulevicius et al. (2016) and with PMF analysis of chemical marker measurements obtained from the same filter samples.

2 Sampling and offline measurements

2.1 Site description and sample collection

We collected 24-h integrated PM₁ filter samples at 3 different stations in Lithuania from 30 September 2013 to 2 September 2014 using 3 High-Volume samplers (Digitel DHA80, and DH-77) operating at 500 L min⁻¹. In order to prevent large negative filter artifacts, the high volume were equipped with temperature control systems maintaining the filter storage temperature always below 25°C, which is lower or comparable to the maximum daily temperature during summer. The particulate matter was collected on 150-mm diameter quartz fiber filters (Pallflex Tissuquartz 2500QAT-UP / pure quartz, no binder) pre-baked at 800°C for 8 h. Filter samples were wrapped in pre-baked aluminum foils (400°C for 6 h), sealed in polyethylene bags and stored at -20°C after exposure. Field blanks were collected and stored following the same procedure.

Sampling was conducted at urban (Vilnius), rural terrestrial (Rūgšteliškis) and rural coastal (Preila) monitoring sites (Fig. 1). The rural terrestrial site of Rūgšteliškis serves as a baseline against which urban-specific sources in the major population center of Vilnius can be

1 compared. The rural coastal site of Preila provides an opportunity to distinguish terrestrial and
2 marine sources.

3 The sampling station in Vilnius is located at the Center for Physical Sciences and Technology
4 campus (54°38' N, 25°10' E, 165 m a.s.l.) 12 km southwest of the city center (population:
5 535000) and is classified as an urban background site. The site is relatively far from busy
6 roads, and surrounded by forests to the north/northeast, and by a residential zone to the
7 south/east. It is ca. 350 km distant from the Baltic coast, and 98 km from the Rūgštelėškis
8 station (Fig. 1).

9 The station in Preila (55°55' N, 21°04' E, 5 m a.s.l.) is a representative rural coastal
10 background site, situated in the Curonian Spit National Park on the isthmus separating the
11 Baltic Sea from the Curonian Lagoon. The monitoring station is located <100 m from the
12 Baltic shore. The closest populated area is the village of Preila (population: 200 inhabitants),
13 located 2 km to the south.

14 The rural terrestrial station of Rūgštelėškis (55°26' N and 26°04' E, 170 m a.s.l.) is located in
15 the eastern part of Lithuania, about 350 km from the Baltic Sea. The site is surrounded by
16 forest and borders the Utenas Lake in the southwest. The nearest residential areas are
17 Tauragnai, Utena (12 km and 26 km west of the station, population: 32000 inhabitants) and
18 Ignalina (17 km southeast of the station, population: 6000 inhabitants).

19 **2.2 Offline-AMS analysis**

20 The term *offline-AMS* will be used herein to refer to the methodology described by
21 Daellenbach et al. (2016) and summarized below. For each analyzed filter sample, four 16-
22 mm diameter filter punches were subjected to ultrasonic extraction in 15 mL of ultrapure
23 water (18.2 MΩ cm at 25°C, total organic carbon (TOC) < 3 ppb) for 20 min at 30°C.

24 The choice of water instead of an organic solvent is motivated by two arguments:

- 25 - Water yields the lowest background and hence the highest signal to noise compared to
26 other highly pure solvents (including methanol, dichloromethane and ethyl acetate).
- 27 - In contrast to the water extraction, the use of organic solvents precludes the
28 quantification of the organic content in the extracts (e.g. by using a total OC analyzer),
29 which in turn prevents a quantitative source apportionment.

1 Liquid extracts were then filtered and atomized in Ar ($\geq 99,998$ % Vol. abs., Carbagas, CH-
2 3073 Gümligen, Switzerland) using an Apex Q nebulizer (Elemental Scientific Inc., Omaha
3 NE 68131 USA) operating at 60°C. The resulting aerosol was then dried by passing through a
4 Nafion drier (Perma Pure, Toms River NJ 08755 USA), and subsequently analyzed by a HR-
5 ToF-AMS. 12 mass spectra per filter sample were collected (AMS V-mode, m/z 12-232, 30 s
6 collection time per spectrum). A measurement blank was recorded before and after each
7 sample by nebulizing ultrapure water for 12 minutes. Field blanks were measured following
8 the same extraction procedure as the collected filter samples, yielding a signal not statistically
9 different from that of nebulized milliQ water. Finally we registered the AMS fragmentation
10 spectrum of pure gaseous CO₂ ($\geq 99,7$ % Vol, Carbagas, CH-3073 Gümligen, Switzerland), in
11 order to derive its CO₂⁺:CO⁺ ratio.

12 Offline-AMS analysis was performed on 177 filter samples in order to determine the bulk
13 water-soluble organic matter (WSOM) mass spectral fingerprints. In total, 63 filters from
14 Rūgšteliškis, 42 from Vilnius, and 71 from Preila were measured in Ar. The reader is referred
15 to DeCarlo et al. (2006) for a thorough description of the AMS operating principles and
16 calibration procedures.

17 HR-ToF-AMS analysis software SQUIRREL (SeQUential Igor data RetRiEvaL, D. Sueper,
18 University of Colorado, Boulder, CO, USA) v.1.53G and PIKA (Peak Integration by Key
19 Analysis) v.1.11L for IGOR Pro software package (Wavemetrics, Inc., Portland, OR, USA)
20 were utilized to process and analyze the AMS data. HR analysis of the AMS mass spectra was
21 performed in the m/z range 12-115.

22 **2.3 Supporting measurements**

23 Additional offline analyses were carried out in order to validate and corroborate the offline-
24 AMS source apportionment results. This supporting dataset was also used as input for PM₁
25 source apportionment as discussed below. The complete list of the measurements performed
26 can be found in Table 1 and Table S1. Briefly, major ions were measured by ion
27 chromatography (IC; Jaffrezo et al., 1998); elemental and organic carbon (EC, OC) were
28 quantified by thermal optical transmittance following the EUSAAR2 protocol (Cavalli et al.,
29 2010); water-soluble OC (WSOC) was measured by water extraction followed by catalytic
30 oxidation and non-dispersive infrared detection of CO₂ using a total organic carbon analyzer
31 (Jaffrezo et al., 2005). Organic markers were determined by gas chromatography-mass

1 spectrometry (GC-MS; Golly et al., 2015); high performance liquid chromatography (HPLC)
 2 associated with a fluorescence detector (LC 240 Perkin Elmer) and HPLC-pulsed
 3 amperometric detection (PAD; Waked et al., 2014) for 67 composite samples. Composites
 4 were created merging two consecutive filter samples, but no measurements are available for
 5 Vilnius during summer. Measurements included 18 polycyclic aromatic hydrocarbons
 6 (PAHs), alkanes (C21-C40), 10 hopanes, 13 methoxyphenols, 13 methyl-PAHs (Me-PAHs), 6
 7 sulfur-containing-PAHs (S-PAHs), 3 monosaccharide anhydrides, and 4 monosaccharides
 8 (including glucose, mannose, arabitol, and mannitol). In this work ion concentrations always
 9 refer to the IC measurements.

10 Table 1. Overview of supporting measurements. A complete list of measured compounds can
 11 be found in table S1.

Analytical Method	Measured compounds	Filters measured
IC (Jaffrezo et al., 1998)	Ions	All
	EC/OC	
Thermal optical transmittance using Sunset Lab Analyzer (Birch and Cary, 1996) using EUSAAR2 protocol (Cavalli et al., 2010)		All
TOC analyzer using persulphate oxidation at 100°C of the OM, followed by CO ₂ quantification with a non-dispersive infrared spectrophotometer (Jaffrezo et al., 1998)	WSOC	All
HPLC associated with fluorescence detector (LC 240 Perkin Elmer) (Golly et al., 2015, Besombes et al., 2001)	PAHs (table S1)	67 composite samples
GC-MS (with and without derivatization step) (Golly et al., 2015)	S-PAHs, Me-PAHs, alkanes, hopanes, methoxyphenols, others	67 composite samples

HPLC-PAD, (Waked et al., 2014)	Anhydrous sugars, sugars alcohols, monosaccharides	67 composite samples
Chemiluminescence (Environnement S.A., Model AC31M)	NO _x	Online (Vilnius only)

1 In the following, subscripts *avg*, and *med* will denote average and median values,
2 respectively.

3 **3 Source apportionment**

4 Positive matrix factorization (PMF, Paatero and Tapper, 1994) is a bilinear statistical model
5 used to describe the variability of a multivariate dataset as the linear combination of a set of
6 constant factor profiles and their corresponding time series, as shown in Eq. (1):

$$7 \quad x_{i,j} = \sum_{z=1}^p (g_{i,z} \cdot f_{z,j}) + e_{i,j} \quad (1)$$

8 Here x , g , f , and e denote elements of data, factor time series, factor profiles and residual
9 matrices, respectively, while subscripts i, j and z are indices for time, measured variables, and
10 factor number. The value p represents the total number of factors chosen for the PMF
11 solution. The PMF algorithm iteratively solves Eq. (1) by minimizing the objective function
12 Q , defined in Eq. (2) Only non-negative $g_{i,z}$ and $f_{z,j}$ values are permitted:

$$13 \quad Q = \sum_i \sum_j \left(\frac{e_{i,j}}{s_{i,j}} \right)^2 \quad (2)$$

14 Here the $s_{i,j}$ elements represent entries in the input error matrix.

15 In this work the PMF algorithm was run in the robust mode in order to dynamically
16 downweigh the outliers. The PMF algorithm was solved using the multilinear engine-2 (ME-
17 2) solver (Paatero, 1999), which enables an efficient exploration of the solution space by a
18 *priori* constraining the $g_{i,z}$ or $f_{z,j}$ elements within a certain variability defined by the scalar a
19 ($0 \leq a \leq 1$) such that the modelled $g_{i,z}'$ and $f_{z,j}'$ satisfy Eq. (3):

$$20 \quad \frac{(1-a)f_{z,n}}{(1+a)f_{z,m}} \leq \frac{f_{z,n'}}{f_{z,m'}} \leq \frac{(1+a)f_{z,n}}{(1-a)f_{z,m}} \quad (3)$$

Here n and m are any two arbitrary columns (variables) in the normalized F matrix. The Source Finder toolkit (SoFi, Canonaco et al., 2013, v.4.9) for Igor Pro software package (Wavemetrics, Inc., Portland, OR, USA) was used to configure the ME-2 model and for post-analysis. PMF analysis was applied to two complementary datasets: (1) organic mass spectra from offline-AMS measurements for the apportionment of OM sources and (2) molecular markers for the apportionment of the measured PM₁ mass. These two analyses are discussed separately below.

3.1 Offline-AMS PMF

In the following section we describe the offline-AMS source apportionment implementation, optimization and uncertainty assessment. Briefly, we selected the number of PMF factors based on residual analyses and solution interpretability; subsequently we explored the rotational uncertainty of our source apportionment model and discarded suboptimal solutions providing insufficient correlation of factor time series with external tracers.

The offline-AMS source apportionment returns the water soluble PMF factor concentrations. Daellenbach et al. (2016) determined factor specific recoveries (including PMF factor extraction efficiencies), by comparing offline-AMS and online-ACSM OA source apportionments. In that work, filter samples were collected for one year during an online-ACSM monitoring campaign conducted at the same sampling station. Briefly, the factor recoveries were determined as the ratio between the water soluble OA PMF-factor concentrations from offline-AMS source apportionment divided by the OA PMF factor concentrations obtained from ACSM source apportionment. Factor specific recoveries and corresponding uncertainties were determined for HOA, BBOA, COA, and OOA. In this work we applied the factor recoveries from Daellenbach et al. (2016) to scale the water soluble factor concentrations retrieved from offline-AMS PMF to the corresponding bulk OA concentrations. We conducted a sensitivity analysis on the applied recoveries (Section 3.1.3), and the corresponding uncertainty was propagated to the source apportionment results. A second solution selection step was carried out on the rescaled solutions as described in section 3.1.3.

In general, the offline-AMS technique assesses less precisely the contribution of the low water soluble factors. The higher uncertainty mostly stems from the larger PMF rotational

ambiguity when separating factors characterized by low concentration in the filter extracts (i.e. low water solubility). Nevertheless, the uncertainty is dataset dependent, as the separation of such sources can be improved in case of distinct time variability of these sources. The low aqueous concentration of scarcely water soluble sources in fact can be partially overcome by the large signal/noise characterizing the offline-AMS technique (170 on average for this dataset).

The offline-AMS source apportionment results presented in this study represent the average of the retained rescaled PMF solutions, while their variability represents our best estimate of the source apportionment uncertainty.

3.1.1 Inputs

The offline-AMS input matrices include in total 177 filter samples (62 filters from Rūgštelis, 42 from Vilnius, and 73 from Preila). Each filter sample was represented on average by 12 mass spectral repetitions to explore the effect of AMS and nebulizer stability on PMF outputs. A corresponding measurement blank was subtracted from each mass spectrum. The input PMF matrices included 269 organic fragments fitted in the mass range (12-115). The input error $s_{i,j}$ elements include the blank variability ($\sigma_{i,j}$) and the uncertainty related to ion counting statistic and ion-to-ion signal variability at the detector ($\delta_{i,j}$, Allan et al., 2003; Ulbrich et al., 2009):

$$s_{i,j} = \sqrt{\delta_{i,j}^2 + \sigma_{i,j}^2} \quad (4)$$

We applied a minimum error to the $s_{i,j}$ matrix elements according to Ulbrich et al. (2009), and a down-weighting factor of 3 to all fragments with an average signal to noise lower than 2 (Ulbrich et al., 2009). Input data and error matrices were rescaled such that the sum of each row is equal to the estimated WSOM concentration, which is calculated as the product of the measured WSOC multiplied by the OM:OC_i ratios determined from the offline-AMS PMF results.

3.1.2 Overview of retrieved factors and estimate of traffic exhaust OA (TEOA)

We used a 4-factor solution to represent the variability of the input data. The 4 separated OA factors included the following:

1 1/ a biomass burning OA (BBOA) factor highly correlated with levoglucosan originating from
2 cellulose pyrolysis;

3 2/ a local OA (LOA) factor explaining a large fraction of N-containing fragments variability
4 and contributing mostly in Vilnius during summer and spring;

5 3/ a background oxygenated-OA (B-OOA) factor showing relatively stable contributions at all
6 seasons;

7 4/ a summer-OOA (S-OOA) factor showing increasing concentrations with the average daily
8 temperature.

9 If the number of factors is decreased to 3, a mixed BBOA/B-OOA factor is retrieved, and
10 significant structure appears in the residuals during winter (Fig. S2, S3, S4). Increasing the
11 number of factors to 5 and 6, leads to a splitting of OOA factors that cannot be interpreted in
12 terms of specific aerosol sources/processes (Fig. S2, S3). The further separated OOA factor in
13 the 5-factor solution possibly derived from the splitting of B-OOA; in fact the sum of the
14 newly separated OOA and B-OOA in the 5-factor solution correlated well with the B-OOA
15 time series from the 4-factor solution ($R = 0.93$). Overall, a clear structure removal in the
16 residual time-series was observed until a number of factors equal to 4 (Fig. S4, S5).

17 We also explored a 5-factor solution in which a hydrocarbon-like OA (HOA) profile from
18 Mohr et al. (2012) was constrained to estimate the TEOA contribution. However, the water-
19 soluble TEOA (WSTEOA) contribution to WSOM was estimated as $0.2\%_{\text{avg}}$ (section 3.1.4),
20 likely too small for PMF to resolve. We performed 100 PMF runs by randomly varying the
21 HOA α -value. The obtained results showed a low TEOA correlation with hopanes ($R_{\text{max}} =$
22 0.25 , $R_{\text{min}} = -0.15$) with 45% of the PMF runs associated with negative Pearson correlation
23 coefficients, supporting the hypothesis that this factor has too small contribution in the water
24 extracts to be resolved. Therefore, we selected the 4-factor solution as our best representation
25 of the data, while TEOA was instead estimated by a chemical mass balance (CMB) approach
26 and not based on AMS mass spectral features.

27 TEOA concentrations are estimated using a CMB approach that assumes hopanes, present in
28 lubricant oils engines, (Subramanian et al., 2006) to be unique tracers for traffic. However,
29 hopanes can also be emitted upon combustion of different types of fossil fuel, in particular by
30 coal combustion (Rutter et al., 2009), therefore the traffic contribution estimated here,
31 although very small (as discussed in the result section) should be considered as an upper

estimate. Still, the EC:hopanes ratio determined in this work (900 ± 100) is consistent with EC:hopanes for TE (1400 ± 900 : He et al., 2006; He et al., 2008; El Haddad et al., 2009; Fraser et al., 1998) and not with the coal EC:hopanes from literature profiles (300 ± 200 : Huang et al., 2014; supplementary information (SI)). To assess the traffic exhaust OC (TEOC) contribution we used the sum of the four most abundant hopanes (17a(H),21b(H)-norhopane, 17a(H),21b(H)-hopane, 22S,17a(H),21b(H)-homohopane, and 22R,17a(H),21b(H)-homohopane (hopanes_{sum})). The TEOC contribution was estimated from the average hopanes_{sum}:TEOC ratio (0.0012 ± 0.0005) from tunnel measurements reported by He et al. (2006), He et al. (2008), El Haddad et al. (2009), and Fraser et al. (1998), where the four aforementioned hopanes were also the most abundant. In order to rescale TEOC to the total TEOA concentration we assumed an OM:OC_{TEOA} ratio of 1.2 ± 0.1 (Aiken et al., 2008, Mohr et al., 2012, Docherty et al., 2011, Setyan et al., 2012). The uncertainty of the estimated TEOA concentration was assessed by propagating the uncertainties relative to the OM:OC_{TEOA} ratio (8.3%), the hopanes_{sum}:TEOC ratio (41.7%), the hopane measurement repeatability (11.5%), and detection limits (7 pg m^{-3}).

3.1.3. Source apportionment uncertainty

A common issue in PMF is the exploration of the rotational ambiguity, here addressed by performing 100 PMF runs initiated using different input matrices. We adopted a bootstrap approach (Davison and Hinkley, 1997) to generate the new input data and error matrices (Brown et al., 2015). Briefly, the bootstrap algorithm generates new input matrices by randomly resampling mass spectra from the original input matrices. As already mentioned, the input matrices contained ca. 12 mass spectral repetitions per filter sample; therefore the bootstrap approach was implemented in order to resample random filter sample mass spectra together with the corresponding measurement repetitions. Each newly generated PMF input matrix had a total number of samples equal to the original matrices (177 samples), although some of the original 177 filter samples are represented several times, while others are not represented at all. Overall we resampled on average $63\pm2\%$ of the filter samples per bootstrap run. The generated data matrices were finally perturbed by varying each $x_{i,j}$ element within twice the corresponding uncertainty ($s_{i,j}$) assuming a normal distribution of the errors. Solutions were selected and retained according to three acceptance criteria based on PMF factor correlations with corresponding tracers: BBOA vs. levoglucosan, B-OOA vs. NH_4^+ ,

and S-OOA vs. average daily temperature. In order to discard suboptimal PMF runs, we only retained solutions associated with positive Pearson correlation coefficients for each criterion, for both the individual stations and the entire dataset. In total 95% of the solutions were retained following this approach. We note that no solution was discarded based on the first two criteria.

The offline-AMS PMF analysis provides the water-soluble contribution of the identified aerosol sources. In order to rescale the water-soluble organic carbon concentration of a generic factor z (WSZOC) to its total OC concentration (ZOC) we used the factor recoveries (R_Z) determined by Daellenbach et al. (2016) according to Eq. (5):

$$ZOC_i = \frac{WSZOC_i}{R_Z} \quad (5)$$

For each PMF factor (BBOA, W-OOA, and S-OOA), the water-soluble organic carbon contribution was determined from the OM:OC ratio calculated from the (water-soluble) factor mass spectrum (Aiken et al. 2008). For LOA, whose recovery was not previously reported, R_{LOA} was estimated from a single parameter fit according to Eq. (6)

$$OC = TEOC + \frac{WSBBOA}{(OM:OC)_{WSBBOA} \cdot R_{BBOA}} + \frac{WSW-OOA}{(OM:OC)_{WSS-OOA} \cdot R_{OOA}} + \frac{WSS-OOA}{(OM:OC)_{WSB-OOA} \cdot R_{OOA}} + \frac{WSLOA}{(OM:OC)_{LOA} \cdot R_{LOA}} \quad (6)$$

Here the water-soluble OA factor concentrations were converted to the corresponding water-soluble OC concentrations to fit the measured OC. For each of the 95 retained PMF solutions, Eq. (6) was fitted 100 times by randomly selecting a set of 100 R_{BBOA} , R_{OOA} combinations from those determined by Daellenbach et al. (2016). Each fit was initiated by perturbing the input OC_i and $TEOC_i$ within their uncertainties, assuming a normal distribution of the errors. Additionally we also perturbed the OC and WSOC inputs in order to explore the effect of possible bulk extraction efficiency (WSOC:OC) systematic biases on our R_Z estimates. Specifically, we assumed an estimated accuracy bias of 5% for each of the perturbed parameters, which corresponds to the OC and WSOC measurement accuracy. In a similar way, we also perturbed the input R_{BBOA} and R_{OOA} assuming an accuracy estimate of 5% deriving from a possible OC measurement bias in Daellenbach et al. (2016) which could have affected the R_Z determination. In total $9.5 \cdot 10^3$ fits were performed (Eq. 6) and we retained only solutions (and corresponding perturbed R_Z combinations) associated with average OC residuals not statistically different from 0 within 1σ for each station individually and for summer and winter individually ($\sim 8\%$ of the $9.5 \cdot 10^3$ fits, Fig. S6). The OC residuals of the accepted solutions did not manifest a clear correlation with the LOA concentration (Fig. S7),

1 indicating that the estimated R_{LOA} was properly fitted, without compensating for unexplained
2 variability of the PMF model or biases from the other R_z . Fig. S8 shows the probability
3 density functions (PDF) of the retained perturbed R_z which account for all uncertainties and
4 biases mentioned above. $R_{LOA,med}$ was estimated to be equal to 0.66 (1st quartile 0.61, 3rd
5 quartile 0.69, Fig. S8), while the retained R_{BBOA} and R_{OOA} values ($R_{BBOA,med}$ 0.57, 1st quartile
6 0.55, 3rd quartile 0.60; $R_{OOA,med}$ 0.84, 1st quartile 0.81, 3rd quartile 0.88) were systematically
7 lower than those reported by Daellenbach et al. (2016), reflecting the lower bulk extraction
8 efficiency (bulk EE = WSOC:OC) measured for this dataset (median = 0.59, 1st quartile =
9 0.51, 3rd quartile = 0.72 vs. median = 0.74, 1st quartile = 0.66, 3rd quartile 0.90 in Daellenbach
10 et al. (2016)). All the retained R_k combinations are available at DOI: doi.org/10.5905/ethz-
11 1007-53.

12 Source apportionment uncertainties ($\sigma_{S,A}$) were estimated for each sample i and factor z as the
13 standard deviation of all the retained PMF solutions ($\sim 8\%$ of the $9.5 \cdot 10^3$ fits). In addition to
14 the rotational ambiguity of the PMF model (explored by the bootstrap technique) and R_Z
15 uncertainty, each PMF solution included on average 10 repetitions for each filter sample, and
16 hence $\sigma_{S,A}$ accounted also for measurement repeatability. In this work, the statistical
17 significance of a factor contribution is calculated based on $\sigma_{S,A,z,i}$ (Tables S2 and S3).

18 In general the recovery estimates reported in Daellenbach et al. (2016) represent the most
19 accurate estimates available, being constrained to match the online-ACSM source
20 apportionment results. The R_Z combinations reported by Daellenbach et al. (2016)
21 demonstrated to positively apply to this dataset, enabling properly fitting the measured Bulk
22 EE (WSOC:OC) with unbiased residuals and therefore providing a further confidence on their
23 applicability (we note that in Eq. 6 we fitted OC as function of $(R_Z)^{-1}$ and $WSOC_{Z,i}$, therefore
24 R_Z fitted $WSOC:OC = \text{Bulk EE}$). In general further R_Z determinations calculated comparing
25 offline-AMS and online-AMS source apportionments would be desirable in order to provide
26 more robust R_Z estimates. In absence of a-priori R_Z values for specific factors (e.g. for LOA in
27 this study) we recommend constraining the R_Z combinations reported by Daellenbach et al.
28 (2016) as a-priori information to fit the unknown recoveries, with the caveat that the R_Z
29 combinations reported by Daellenbach et al. (2016) were determined for filter samples
30 extracted with water following a specific procedure; therefore we recommend adopting these
31 R_Z combinations for filter samples extracted in the same conditions. Nevertheless the R_Z
32 combinations reported by Daellenbach et al. (2016) should be tested also for filters water

1 extracted in different conditions to verify whether they can properly fit the Bulk EE. In case
2 the R_Z combinations reported by Daellenbach et al. (2016) would not apply for a specific
3 location or extraction procedure (i.e. not enabling a proper fit of Bulk EE) we recommend a
4 R_Z redetermination by comparing the offline-AMS source apportionment results with well-
5 established source apportionment techniques. In absence of data to perform a well-established
6 source apportionment, we recommend to fit all the R_Z to match the bulk EE (i.e. fitting all the
7 recoveries similarly as in Eq. 6 without constraining any a-priori R_Z value).

9 3.1.4. Sensitivity of PMF to the un-apportioned TEOA fraction

10 Despite representing only a small fraction, the un-apportioned water-soluble TEOA
11 (WSTEOA) contribution could in theory affect the apportionment of the other sources in the
12 PMF model. To assess this, we performed a PMF sensitivity analysis by subtracting the
13 estimated WSTEOA concentration from the input PMF data matrix, and by propagating the
14 estimated WSTEOA uncertainty (section 3.1.2) in the input error matrices. To estimate the
15 WSTEOA concentration we assumed R_{TEOA} of 0.11 ± 0.01 (Daellenbach et al., 2016) and we
16 used the HOA profile reported by Mohr et al. (2012) as surrogate for the TEOA mass spectral
17 fingerprint. This approach is equivalent to constraining both the WSTEOA time series and
18 factor profile. Overall the WSTEOA contribution to WSOM was estimated as $0.2\%_{avg}$,
19 making a successful retrieval of WSTEOA unlikely (Ulbrich et al., 2009). Consistently, PMF
20 results obtained from this sensitivity analysis indicated that BBOA and B-OOA were robust,
21 showing only 1% difference from the average offline-AMS source apportionment results,
22 with BBOA increased and B-OOA decreased. S-OOA and LOA instead showed larger
23 deviations from the average source apportionment results (S-OOA increased by 8% and LOA
24 decreased by 15%), yet within our source apportionment uncertainties. These results highlight
25 the marginal influence of the un-apportioned WSTEOA fraction on the other factors.

27 3.2 Marker-PMF: measured PM_1 source apportionment

28 In the following section we describe the implementation of source apportionment using
29 chemical markers (marker-PMF), as well as its optimization and uncertainty assessment. We
30 discuss the number of factors and the selection of specific constraints to improve the source
31 separation. Subsequently we discuss the source apportionment rotational uncertainty, and the

sensitivity of our PMF results to the number of source specific markers, and to the assumed constraints.

3.2.1 Inputs

The marker-PMF yields a source apportionment of the entire measured PM₁ fraction (organic and inorganic). Measured PM₁ is defined here as the sum of EC, ions measured via IC, and OM estimated from OC measurements multiplied by the (OM:OC)_i ratio determined from the offline-AMS PMF results by summing the factor profiles OM:OC ratios weighted by the time dependent factor relative contributions (rescaled by the recoveries). PMF was used to analyze a data matrix consisting of selected organic molecular markers, ions measured by IC, EC, and the remaining OM fraction (OM_{res}) calculated as the difference between OM and the sum of the organic markers already included in the input matrix. OM_{res} represented on average 95±2% of total OM. The marker-PMF analysis is limited by the lack of elemental measurements (e.g. metals and other trace elements) typically used to identify mineral dust and certain anthropogenic sources. All markers showing concentrations above the detection limits for more than 25% of the samples were selected as input variables (72 in total). The PMF input matrices contain 67 composite samples (31 for Rūgštelīškis, 29 for Preila, and 7 for Vilnius). The errors ($s_{i,j}$) were estimated by propagating for each j variable the detection limits (DL) and the relative repeatability (RR) multiplied by the $x_{i,j}$ concentration according to Eq. (7) (Rocke and Lorenzato, 1995):

$$s_{i,j} = \sqrt{(DL_j)^2 + (x_{i,j} \cdot RR_{i,j})^2} \quad (7)$$

3.2.2 Number of factors and constraints

We selected a 7-factor solution to explain the variability of the measured PM₁ components. The retrieved factors were biomass burning (BB), traffic exhaust (TE), primary biological organic aerosol (PBOA), SO₄²⁻-related secondary aerosol (SA), NO₃⁻-related SA, methane sulfonic acid (MSA)-related SA, and a Na⁺-rich factor explaining the variability of inorganic components typically related to resuspension of mineral dust, sea salt, and road salt.

We first tested an unconstrained source apportionment. This led to a suboptimal separation of the aerosol sources, with large mixings of PMF factors associated with contributions of markers originating from different sources. In particular we observed mixing of BB markers (e.g. levoglucosan) with fossil fuel combustion markers such as hopanes, as well as with

1 inorganic ions such as NO_3^- and Ca^{2+} . All these markers, although related to different
2 emission/formation processes, are characterized by similar seasonal trends, i.e. higher
3 concentrations during winter than in summer. Specifically, the BB tracers increase during
4 winter because of domestic heating activity, hopanes presumably because of the accumulation
5 in a shallower boundary layer and lower photochemical degradation, NO_3^- because of the
6 partitioning into the particle phase at low temperatures, and Ca^{2+} because winter was the
7 windiest season and therefore was associated with the most intense resuspension.

8 We subsequently exploited the markers' source-specificity to set constraints for the profiles
9 output by our model: for each individual source, we treated the contribution of the unrelated
10 source-specific markers as negligible (e.g. we assumed that TE, SA, Na-rich factor and PBOA
11 do not contribute to levoglucosan). In contrast, the non-source specific variables (EC, OM_{res} ,
12 (Me-)PAHs, S-PAHs, inorganic ions, oxalate, alkanes) were freely apportioned by the PMF
13 algorithm. In a similar way we set constraints for primary markers (e.g. K^+ and Ca^{2+}) and
14 combustion related markers (e.g. PAHs), which are not source-specific but the contribution of
15 which can be considered as negligible in the SA factors. In this case the algorithm can freely
16 apportion these markers to all the primary factors and combustion-related factors,
17 respectively.

18 In details, EC, PAHs, and methyl-PAHs were constrained to zero in non-combustion sources,
19 i.e. all profiles but TE and BB. While EC could partially derive from dust resuspension,
20 literature profiles for this source suggest an EC contribution below 1% (Chow et al., 2003).
21 This is expected to be also the case here given the distance of the three stations from
22 residential areas and busy roads. Methoxyphenols and sugar anhydrides, considered to be
23 unique BB markers, were constrained to zero in all sources but BB. Similarly, hopanes were
24 constrained to zero in all factors but TE. We also assumed no contribution from glucose,
25 arabitol, mannitol, and sorbitol to all secondary factors, and traffic exhaust. The SO_4^{2-}
26 contribution from primary traffic emissions was estimated to be negligible, given the use of
27 desulfurized fuel for vehicles in Lithuania. Likewise, alkane contributions were assumed to be
28 zero in the SA factors, similar to the contribution of Ca^{2+} , Na^+ , K^+ and Mg^{2+} in the SA factors
29 and TE.

30 The number of factors was increased until no mixing between source-specific markers for
31 different aerosol sources/processes was observed any more. Secondary sources instead were
32 explained by three factors because of the distinct seasonal and site-to-site variability of MSA,

1 NO_3^- and SO_4^{2-} . Oxalate correlated well with NH_4^+ ($R=0.62$) and the latter well with the sum
2 of SO_4^{2-} and NO_3^- equivalents ($R=0.98$). Note that the aforementioned secondary tracers were
3 not constrained in any factor with the exception of SO_4^{2-} contributions which were assumed to
4 be negligible in the TE factor. Moreover the 7-factor solution showed unbiased residuals
5 (residual distribution centered at 0 within 1σ) for all the stations together and for each station
6 individually, while lower order solutions showed biased residuals for at least one station or all
7 the stations together.

8 PMF results obtained assuming only the aforementioned constraints returned suboptimal
9 apportionments of OM_{res} and Na^+ between the BB and the Na^+ -rich factor, with unusually
10 high OM_{res} fractional contributions in the Na^+ -rich factor and unusually high Na^+
11 contributions in the BB profile in comparison with literature profiles (Chow et al., 2003;
12 Huang et al., 2014 and references therein; Schauer et al., 2001). Similarly the EC: OM_{res} value
13 for TE was substantially lower than literature profiles (El Haddad et al., 2013 and references
14 therein). Other constraints were therefore introduced to improve the separation of these three
15 variables. Specifically, EC and OM_{res} were constrained in the traffic profile to be equal to
16 0.45 and 0.27 (α -value = 0.5) according to El Haddad et al. (2013), while EC:BB ratio was
17 constrained to 0.1 (α -value = 1) according to Huang et al. (2014) and references therein. Na^+
18 was constrained to 0.2% (α -value = 1) in BB according to Schauer et al. (2001), while OM_{res}
19 was constrained to zero in the Na^+ -rich factor to avoid mixing with BB. Although this
20 represents a strict constraint, we preferred avoiding constraining OM_{res} to a specific value for
21 the Na^+ -rich factor which could not be linked to a unique source but possibly represents
22 different resuspension-related sources (e.g. sea salt, mineral dust and road dust). However, we
23 expect none of the aforementioned sources to explain a large fraction of the submicron OM_{res}
24 (the OC:dust ratio for dust profiles is 1-15% according to Chow et al., 2003). The sensitivity
25 of our source apportionment to the constraints listed in this section is discussed in the next
26 section.

28 3.2.3. Source apportionment uncertainty and sensitivity analyses

29 We explored the model rotational uncertainty by performing 20 bootstrap PMF runs, and by
30 perturbing each input $x_{i,j}$ element within $2 \cdot s_{i,j}$ assuming a normal distribution of the errors.
31 Results and uncertainties of the PMF model reported in this paper represent the average and
32 the standard deviation of the bootstrap runs.

1 As discussed in section 3.2.2, we assumed the contribution of specific markers to be 0 in
2 different factor profiles. Such assumptions preclude the PMF model to vary the contributions
3 of these variables from 0 (Eq. 3). In order to explore the effect of such assumptions on our
4 PMF results we loosened all these constraints assuming variable contributions equal to 50%,
5 37.5%, 25%, and 12.5% of their average relative contribution to measured PM_{10} . In all cases
6 the α -value was set to 1. The average factor concentrations for the 12.5% case and the fully
7 constrained average bootstrap PMF solutions were not statistically different (confidence
8 interval of 95%, Fig. S9). Statistically significant differences arose for the of the SO_4^{2-} -related
9 SA in the 50% and 37.5% cases, and the Na^+ -rich factor in the 25% and 37.5% cases,
10 indicating that loosening the constraints allowed additional rotational uncertainty in
11 comparison to the uncertainty explored by the bootstrap approach. By contrast, the factors
12 associated with large relative uncertainties from the marker source apportionment (TE and
13 PBOA, Table S3) showed the best agreement in terms of concentrations (Fig. S9) with the
14 fully constrained solution, suggesting that the variability introduced by loosening the
15 constraints did not exceed that already accounted for by the bootstrap approach. As previously
16 mentioned, the largest contribution discrepancies were observed for the SO_4^{2-} -related SA and
17 Na^+ -rich factor. Looser constraints increased the explained variability of primary components
18 such as EC, arabitol, sorbitol, K^+ , Mg^{2+} , and Ca^{2+} by the (secondary) SO_4^{2-} -related SA factor.
19 The Na^+ -rich factor showed increasing contributions from OM_{res} and from BB components
20 such as methoxyphenols, and anhydrous sugars, which exhibited similar seasonal trends as the
21 Na^+ -rich factor. None of the marker-PMF factors showed statistically different average
22 contributions (confidence interval of 95%) when tolerating a variability of the constrained
23 variables within 12.5% of their relative contribution to PM_{10} . Note that with this degree of
24 tolerance the contribution of OM to the Na^+ -rich was 28%, which is unrealistically high
25 compared to typically reported values for OM:dust ratios (<15% Chow et al., 2003).
26 Therefore, we consider the fully constrained PMF solution to represent best the average
27 composition of the contributing sources.

28 The marker-PMF source apportionment depends strongly on the input variables (i.e. measured
29 markers), as these are assumed to be highly source specific. That is, minor sources, such as
30 MSA-related SA and PBOA, are separated because source-specific markers were used as
31 model inputs. Meanwhile, more variables were used as tracers for TE and BB
32 (methoxyphenols (5 variables), sugar anhydrides (3 variables), and hopanes (5 variables)),
33 which gives more weight to these specific sources. We explored the sensitivity of the PMF

1 results to the number and the choice of traffic and wood burning markers, by replacing them
2 with randomly selected input variables. In total 20 runs were performed and the average
3 contribution of the different sources to OM_{res} was compared with the marker source
4 apportionment average results, where bootstrap was applied to resample time points. Results
5 displayed in Fig. S10 are in agreement the apportionment of OM_{res} from BB within 11%_{avg},
6 highlighting its robustness. The agreement for TE was lower, which is not surprising given
7 the lower contribution of this source and the smaller number of specific markers (hopanes).
8 However, these uncertainties were within the marker source apportionment uncertainty (Fig.
9 S10), implying that the results were not significantly sensitive to the number and the choice of
10 input markers for BB and traffic exhaust.

11

12 **4 Results and Discussion**

13 **4.1 PM₁ composition**

14 An overview of the measured PM₁ composition can be found in Fig. 1. Measured PM₁
15 average concentrations were in general low, with lower values detected at the rural terrestrial
16 site of Rūgšteliškis ($5.4 \mu\text{g m}^{-3}_{avg}$) than in Vilnius ($6.7 \mu\text{g m}^{-3}_{avg}$) and Preila ($7.0 \mu\text{g m}^{-3}_{avg}$).
17 OM represented the major fraction of measured PM₁ for all seasons and stations, with 57%_{avg}
18 of the mass. The average OM concentrations were higher during winter ($4.2 \mu\text{g m}^{-3}$) than in
19 summer ($3.0 \mu\text{g m}^{-3}$) at all sites probably to a combination of domestic wood burning activity
20 and accumulation of the emissions in a shallower boundary layer. For similar reasons, EC
21 average concentrations showed higher values during winter ($0.42 \mu\text{g m}^{-3}$) than in summer
22 ($0.25 \mu\text{g m}^{-3}$). During summer, the average EC concentration was ~5 times higher in Vilnius
23 ($0.54 \mu\text{g m}^{-3}$) than in Preila and Rūgšteliškis (0.12 and $0.11 \mu\text{g m}^{-3}$, respectively), indicating
24 an enhanced contribution from combustion emissions. In the absence of domestic heating
25 during this period, a great part of these emissions may be related to traffic. During winter, EC
26 concentrations were comparable at all sites (only 25% higher in Vilnius than in Preila and
27 Rūgšteliškis). This suggests that a great share of wintertime EC may be related to BB, the
28 average contribution of which is significant at all stations within 3σ (table S2). It should be
29 noted that the highest measured PM₁ concentrations were detected at the remote rural coastal
30 site of Preila during three different pollution episodes. In particular, the early March episode
31 corresponded to the period analyzed by Ulevicius et al. (2016) and Dudoitis et al. (2016), and

was attributed to regional transport of polluted air masses associated to an intense land clearing activity characterized by large scale grass burning in the neighboring Kaliningrad region. SO_4^{2-} represented the second major component of measured PM_{10} (20%_{med}) at all sites and seasons. Its average concentration remained rather constant with only slightly higher concentrations in summer than in winter ($1.2 \pm 0.7 \mu\text{g m}^{-3}$, and $1.1 \pm 0.6 \mu\text{g m}^{-3}$ respectively). Overall SO_4^{2-} concentrations did not show large differences from site-to-site, suggestive of regional sources. By contrast NO_3^- showed a clear seasonality with larger contributions in winter (average $0.9 \pm 0.8 \mu\text{g m}^{-3}$ equivalent to 12% of measured PM_{10}) than in summer ($0.03 \pm 0.03 \mu\text{g m}^{-3}$), as expected from its semi-volatile nature.

4.2 OM source apportionment (Offline-AMS PMF)

The apportioned PMF factors were associated to aerosol sources/processes according to their mass spectral features, seasonal contributions and correlations with tracers. The four identified factors were BBOA, LOA, B-OOA, and S-OOA, which are thoroughly discussed below. The TEOA contributions instead were determined using a CMB approach.

BBOA was identified by its mass spectral features, with high contributions of $\text{C}_2\text{H}_4\text{O}_2^+$, and $\text{C}_3\text{H}_5\text{O}_2^+$ (Fig. 2), typically associated with levoglucosan fragmentation from cellulose pyrolysis (Alfarra et al., 2007), accordingly the BBOA factor time series correlated well with levoglucosan (Pearson correlation coefficient: $R=0.90$, Fig. S11). BBOA contributions were higher during winter and lower during summer (Fig. 3a). We determined the biomass burning organic carbon (BBOC) concentration from the BBOA time series divided by the $\text{OM}:\text{OC}_{\text{BBOA}}$ ratio determined from the corresponding HR spectrum. The winter levoglucosan:BBOC ratio was 0.16_{med}, consistent with values reported in continental Europe for ambient BBOC profiles (levoglucosan:BBOC range: 0.10-0.21, Zotter et al., 2014; Minguillón et al., 2011; Herich et al., 2014).

The second factor was defined as LOA because of its statistically significant contribution (within 3σ) only in Vilnius during summer (table S2), in contrast to other potentially local primary (e.g. BBOA) and secondary (S-OOA) sources which contributed at all sites. The LOA mass spectrum was characterized by a high contribution of N-containing fragments (especially $\text{C}_5\text{H}_{12}\text{N}^+$, and $\text{C}_3\text{H}_8\text{N}^+$), with the highest N:C ratio (0.049) among the apportioned PMF factors (0.029 for BBOA, 0.013 for S-OOA, 0.023 for B-OOA). A similar factor was also observed by Byčenkienė et al. (2016) using an ACSM at the same station. In that work,

1 high LOA concentrations were associated with wind directions from N-NW, and the authors
2 suggested the sludge utilization system of Vilnius (UAB Vilniausvandenys) situated 3.9 km
3 NW from the sampling station as a probable source.

4 Two different OOA sources (S-OOA and B-OOA) were resolved and exhibited different
5 seasonal trends. Separation and classification of OOA sources from offline-AMS is typically
6 different from that of online AMS and ACSM measurements, mainly due to the different time
7 resolution. Few online-AMS studies reported the separation of isoprene-related OA factor
8 (Budisulistiorini et al., 2013; Hu et al., 2015, Xu et al., 2015) mostly driven by isoprene
9 epoxides chemistry. Xu et al. (2015) showed that nighttime monoterpene oxidation by nitrate
10 radical contributes to less-oxidized OOA. However, the large majority of online-AMS OOA
11 factors are commonly classified based on their volatility (semi-volatile OOA and low-
12 volatility OOA) rather than on their sources and formation mechanisms.

13 This differentiation is typically achieved only for summer datasets when the temperature
14 gradient between day and night is sufficiently high, yielding a detectable daily partitioning
15 cycle of the semi-volatile organic compounds and NO_3^- between the gas and the particle
16 phases. Online AMS datasets have higher time resolution than filter sampling, but sampling
17 periods typically cover only a few weeks. Therefore the apportionment is driven by daily
18 variability rather than seasonal differences. By contrast, in the offline-AMS source
19 apportionment, given the 24-h time resolution of the filter sampling and the yearly cycle time
20 coverage, the separation of the factors is driven by the seasonal variability of the sources and
21 by the site-to-site differences. In general, OOA factors with different seasonal behaviors can
22 be characterized by different volatilities. However in this work the offline-AMS OOA
23 separation is not driven by volatility, given the low correlation between NO_3^- and our OOA
24 factors (also reflected by the low NO_3^- -related SOA correlation with B-OOA and S-OOA,
25 Table 2). Additionally, the partitioning of semi-volatile OA at low temperatures would lead to
26 a less oxidized OOA fingerprint during winter than in summer; however, this was not the
27 case. We observed a less oxidized OOA factor during summer, whose mass spectral
28 fingerprint closely resembles that of SOA from biogenic precursors. Meanwhile similar to
29 OOA from aging of biomass burning emissions, OOA during the cold season is more
30 oxidized. This has been also reported in an urban environment in central Europe (Zurich)
31 using an online-ACSM (Canonaco et al., 2015).

Table 2: Pearson correlation coefficients between non-combustion factors (Other-OA components) from offline-AMS and marker-source apportionment.

		Other-OA _{marker}			
		SO ₄ ²⁻ -related SOA	MSA-related SOA	NO ₃ ⁻ -related SOA	PBOA
Other-OA _{offline-AMS}	LOA	0.33	0.16	-0.08	0.10
	B-OOA	0.70	0.22	0.21	0.47
	S-OOA	0.60	0.45	-0.47	0.05

The resolved B-OOA factor explained a higher fraction than S-OOA. It was associated with background oxygenated aerosols as no systematic seasonal pattern was observed. However, B-OOA correlated well with NH₄⁺ ($R=0.69$, Fig. S11), and had the highest OM:OC ratio among the apportioned PMF factors (2.21).

Unlike B-OOA, S-OOA showed a clear seasonality with higher contributions during summer, increasing exponentially with the average daily temperature (Fig. S12a). During summer the site-to-site S-OOA concentrations were not statistically different within a confidence interval of 95%, while during winter the site-to-site agreement was lower, possibly due to the larger model uncertainty associated with the low S-OOA concentrations. A similar S-OOA vs. temperature relationship was reported by Leaitch et al. (2011) for a terpene dominated Canadian forest using an ACSM and by Daellenbach et al. (2016) and Bozzetti et al. (2016) for the case of Switzerland (Fig. S12b), using a similar source apportionment model. This increase in S-OOA concentration with temperature is consistent with the exponential increase in biogenic SOA precursors (Guenther et al., 2006). Therefore, even though the behavior of S-OOA at different sites might be driven by several parameters, including vegetation coverage, available OA mass, air masses photochemical age and ambient oxidation conditions (e.g. NO_x concentration), temperature seems to be the main driver of S-OOA concentrations. Overall more field observations at other European locations are needed to validate this relation. While the results indicate a probable secondary biogenic origin of the S-OOA factor, the precursors of the B-OOA factor are not identified. In section 4.4.2 more insights into the OOA sources will be discussed.

The S-OOA profile showed a CO₂⁺:C₂H₃O⁺ ratio of 0.61_{avg}, placing it in the region of semi-volatile SOA from biogenic emissions in the f_{44}/f_{43} space (Ng et al., 2011), as attributed by Canonaco et al. (2015). Despite the higher summer photochemical activity, the water-soluble bulk OA showed more oxidized mass spectral fingerprints during winter (O:C=0.61_{avg}) than

1 in summer ($\text{O:C}=0.55_{\text{avg}}$), similar to the results presented by Canonaco et al. (2015) for
2 Zurich. Accordingly, the S-OOA profile also showed a less oxidized water-soluble mass
3 spectral fingerprint than B-OOA, with an O:C ratio of 0.40_{avg} , in comparison with 0.80_{avg} for
4 B-OOA. Considering the sum of B-OOA and S-OOA, the median OOA: NH_4^+ ratios for
5 Rūgštelis, Preila, and Vilnius were 3.2, 2.4, and 2.5 respectively, higher than the average
6 but within the range of the values reported by Crippa et al. (2014) for 25 different European
7 rural sites (2.0_{avg} ; minimum value 0.3; maximum 7.3).

9 **4.3 PM₁ source apportionment (marker-PMF)**

10 The PMF factors in this analysis were associated with specific aerosol sources/processes
11 according to their profiles, seasonal trends and relative contributions to the key variables. Fig.
12 4 displays factor profiles, and the relative contribution of each factor to each variable. The
13 Na^+ -rich factor explained a large part of the variability of Ca^{2+} , Mg^{2+} , and Na^+ (Fig. 4) and
14 showed higher contributions during winter than in summer (Fig. 5), suggesting a possible
15 resuspension of sand and salt typically used during winter in Lithuania for road de-icing. This
16 seasonal trend is also consistent with wind speed, which showed the highest monthly values
17 during December 2013 and January 2014. We cannot exclude the possibility that this factor
18 may include contributions from sea salt, although Na^+ and Cl^- were not enhanced at the
19 marine station in comparison with the other stations. The overall contribution of this Na^+ -rich
20 factor to measured PM₁ was relatively small ($1\%_{\text{avg}}$), but may be larger in the coarse fraction.

21 The BB factor showed a well-defined seasonality, with high contributions during winter. This
22 factor explained a large part of the variability of typical wood combustion tracers such as
23 methoxyphenols, sugar anhydrides (including levoglucosan, mannosan, and galactosan), K^+ ,
24 Cl^- , EC, PAHs, and methyl-PAHs (Fig. 4). Using the OM:OC_{BBOA} ratio (1.88) calculated
25 from offline-AMS, we estimated the levoglucosan:BBOC ratio to be 0.18_{avg} , which is within
26 the range of previous studies (Ulevicius et al., 2016 and references therein). Note that this
27 factor explained also large fractions of variables typically associated with non-vehicular fossil
28 fuel combustion, such as benzo(b)naphtho(2,1-d)thiophene (BNT[2,1]) and 6,10,14-trimethyl-
29 2-pentadecanone (DMPT, Fig. 4, Manish et al., 2007; Subramanian et al., 2007), indicating a
30 potential mixing of BB with fossil fuel combustion sources. However, the fossil fuel
31 combustion contribution to BB is unlikely to be large, considering the low concentrations of
32 fossil fuel tracers such as hopanes (66% of the samples below quantification limit ($<\text{QL}$)),

1 BNT[2,1] (64%<QL), and DMPT (55%<QL). Moreover, the above mentioned agreement of
2 the levoglucosan:BBOC ratio with previous studies corroborates the BB estimate from the
3 marker-PMF.

4 The traffic exhaust factor explained a significant fraction of the alkane variability, with a
5 preferential contribution from light alkanes (Fig. 4). Its contribution was never statistically
6 significant within 3σ . However on average the concentration was higher in Vilnius than at the
7 other stations and in general higher in winter than in summer.

8 The PBOA factor explained the variability of the primary biological components, such as
9 glucose, mannitol, sorbitol, arabitol, and alkanes with an odd number of carbon atoms
10 (consistent with Bozzetti et al., 2016 and references therein). Highest PBOA concentrations
11 were observed during spring, especially at the rural site of Rūgštelis. Overall the
12 contribution of this factor was uncertain with an average relative model error of 160%
13 probably due to the small PBOA contributions ($0.6\%_{\text{avg}}$ of the total OM), which hampers a
14 more precise determination by the model. In particular OM_{res} was the variable showing the
15 highest mass contribution to the PBOA factor. However, the large contribution and the large
16 uncertainty of OM_{res} to this factor (0.3 ± 0.4) resulted in a large uncertainty in the PBOA
17 estimated concentration.

18 The last three factors were related to SA, as indicated by the large contributions of secondary
19 species such as oxalate, SO_4^{2-} , MSA, and NO_3^- to the factor profiles (Fig. 4). The three factors
20 showed different spatial and temporal contributions.

21 The NO_3^- -related SA exhibited highest contributions during winter, suggesting temperature-
22 driven partitioning of secondary aerosol components. Moreover the NO_3^- -related SA,
23 similarly to BB and TE, showed the highest concentrations in Vilnius, and the lowest in
24 Rūgštelis suggesting its possible relation with anthropogenic gaseous precursors (e.g.
25 NO_x), as already reported in other studies (e.g. Xu et al., 2016; McMeeking et al., 2012).

26 The MSA-related SA factor manifested the highest concentrations at the marine site of Preila
27 during summer, and in general larger contributions during summer than winter, suggesting its
28 relation with marine secondary aerosol. MSA has been reported to be related to marine
29 secondary biogenic emissions deriving from the photo-oxidation of dimethyl sulfide (DMS)
30 emitted by the phytoplankton bloom occurring during the warm season (Li et al., 1993,
31 Crippa et al., 2013 and references therein).

The last factor (SO_4^{2-} -related SA) showed higher contributions during summer than in winter without clear site-to-site variability, following the seasonal behavior of SO_4^{2-} showing slightly higher concentrations during summer than in winter, which is probably driven by the secondary formation from gaseous photochemical reactions and aqueous phase oxidation. This factor explained the largest part of the oxalate and SO_4^{2-} variability and represented 48%_{avg} of the measured PM_1 by mass.

4.4 Comparison of the source apportionment methods

In this section we compare the offline-AMS PMF and marker-PMF results. We begin with BBOA and TEOA emissions which were resolved by marker-PMF and offline-AMS (TEOA was not resolved by offline-AMS but determined through a CMB approach). The remaining OM fraction (Other-OA = OA – BBOA - TEOA) was apportioned by the offline-AMS source apportionment to B-OOA, S-OOA and LOA (Other-OA_{offline-AMS}). However, the LOA contribution was statistically significant (within 3σ) only in Vilnius during summer (Table S2), while no data were available for these periods from the marker source apportionment. The marker source apportionment instead attributed the Other-OA mass fraction to 4 factors (Other-OA_{marker}): PBOA, as well as to SO_4^{2-} , NO_3^- , and MSA-related secondary organic aerosols (SOA, Fig. S13). The OA concentrations of the factors retrieved from the PM_1 markers source apportionment were obtained by multiplying the factor time series by the sum of the organic markers and OM_{res} contributions to the normalized factor profiles. The PM concentrations from the marker PMF factors are displayed in Fig. 5.

4.4.1 Primary OA sources

Offline-AMS and marker source apportionments provided comparable BBOA estimates, with concentrations agreeing within a 95% confidence interval (Fig. 6). Results revealed that BBOA contributed the largest fraction to the total OM during winter in Preila and Vilnius, while in Rūgšteliškis the largest OA source derived from B-OOA. The average winter BBOA concentration was $1.1 \pm 0.8 \mu\text{g m}^{-3}$ in Rūgšteliškis and $2 \pm 1 \mu\text{g m}^{-3}$ in Vilnius (errors in this section represent the standard deviation of the temporal variability). Overall the average BBOA concentrations were higher at the urban background site of Vilnius and lower at the rural terrestrial site of Rūgšteliškis. Preila showed higher values ($3 \pm 3 \mu\text{g m}^{-3}$) driven by the grass burning episode occurred at the beginning of March (Ulevicius et al., 2016). Excluding this episode, the BBOA winter concentration was lower than in Vilnius ($1.8 \mu\text{g m}^{-3}$). During

1 winter, considering only the samples concomitantly collected, Preila and Vilnius showed well
2 correlated BBOA time series ($R = 0.91$) and significantly positive correlations were observed
3 for also for Preila and Rūgštelis ($R = 0.72$) and for Vilnius and Rūgštelis ($R = 0.66$)
4 (offline-AMS BBOA time series). These results highlight the effect of regional
5 meteorological conditions on the BBOA daily variability in the south east Baltic region.

6
7 By contrast, during summer BBOA concentrations were much lower, with 40% of the points
8 showing statistically not significant contributions within 3σ for the offline-AMS source
9 apportionment and 100% for the marker source apportionment. Between late autumn and
10 early March the offline-AMS source apportionment revealed three simultaneous episodes
11 with high BBOA concentrations at the three stations, while the marker source apportionment
12 which is characterized by lower time resolution did not capture some of these episodes. The
13 first episode occurred between 19 and 25 December 2013 during a cold period with an
14 average daily temperature drop to $-9.7\text{ }^{\circ}\text{C}$ as measured at the Rūgštelis station (no
15 temperature data were available for the other stations). The third episode occurred between 5
16 and 10 March 2014 and was associated with an intense grass burning episode localized mostly
17 in the Kaliningrad region (Ulevicius et al., 2016, Dudoitis et al., 2016, Mordas et al., 2016).
18 The episode was not associated with a clear temperature drop, with the highest concentration
19 ($14\text{ }\mu\text{g m}^{-3}$) found at Preila on 10 March 2014, the closest station to the Kaliningrad region.
20 Similarly, at the beginning of February high BBOA concentrations were registered at the
21 three stations, without a clear temperature decrease. Other intense BBOA events were
22 detected but only on a local scale, with intensities comparable to the regional scale episodes.
23 Using the OM:OC_{BBOA} ratio calculated from the HR water-soluble BBOA spectrum (1.88),
24 we estimated the BBOC_{avg} concentrations during the grass burning episode (5-10 March
25 2014) to span between 0.8 and $7.2\text{ }\mu\text{g m}^{-3}$. On a daily basis our BBOC concentrations are
26 consistent with the estimated ranges reported by Ulevicius et al. (2016) for non-fossil primary
27 organic carbon (0.6 - $6.9\text{ }\mu\text{g m}^{-3}$ during the period under consideration), showing also a high
28 correlation ($R=0.98$).

29 TEOA estimates obtained by CMB and marker-PMF always agreed with each other within 3σ
30 (Fig. 6). The two approaches confirm that TEOA is a minor source at all three stations (Fig.
31 6), consistently, hopanes concentrations (used in this work as TEOA tracers) were below
32 detection limits (7 pg m^{-3}) for 66% of the collected samples. Similarly to NO_x , hopanes,

1 showed a clear spatial and seasonal variability with higher concentrations in Vilnius during
2 winter, suggesting an accumulation of traffic emissions in a shallower boundary layer (Fig.
3 3b, NO_x data available only for Vilnius). During the grass burning event, we observed a peak
4 in the total hopane concentration, and therefore also a peak of the estimated TEOA (2.4 µg m⁻³
5 maximum value). This relatively high concentration is most probably not due to a local
6 increase of TE, but rather due to a regional transport of polluted air masses from neighboring
7 countries (Poland and the Russian Kaliningrad enclave). By assuming an OM:OC_{TEOA} ratio of
8 1.2±0.1 (Aiken et al., 2008, Mohr et al., 2008, Docherty et al., 2011, Setyan et al., 2012), we
9 determined the corresponding organic carbon content (TEOC). Our TEOC concentration was
10 consistent within 3σ with the average fossil primary OC over the whole episode estimated by
11 Ulevicius et al. (2016), (0.4-2.1 µg m⁻³) although on a daily basis the agreement was relatively
12 poor.

13 Overall, offline-AMS source apportionment and marker-PMF returned comparable results for
14 BBOA and similarly the TEOA estimate by markers-PMF and CMB were comparable,
15 therefore not surprisingly the offline-AMS and marker-PMF approaches yielded OA
16 concentrations also for the Other-OA fractions which agreed within 3σ.

17 4.4.2 Other-OA sources: offline-AMS and marker-source apportionment 18 comparison

19 The marker-source apportionment, in comparison to the offline-AMS source apportionment
20 enables resolving well-correlated sources (e.g. BBOA and NO₃⁻-related SOA) as well as
21 minor sources (e.g. MSA-related SOA and PBOA) because source-specific markers were
22 used as model inputs. By contrast, the offline-AMS source apportionment is capable of
23 resolving OA sources for which no specific markers were available such as LOA, which was
24 separated due to the distinct spatial and temporal trends of some N-containing AMS
25 fragments. We first briefly summarize the Other-OA factor concentrations and their site-to-
26 site differences retrieved by the two techniques; subsequently we compare the two source
27 apportionment results.

28 The Other-OA_{offline-AMS} factor time series are displayed in Fig. S13. The B-OOA factor
29 showed relatively stable concentrations throughout the year with 0.9±0.8_{avg} µg m⁻³ during
30 summer and 1.1±0.9_{avg} µg m⁻³ during winter. Although B-OOA concentrations were relatively
31 stable throughout the year, higher contributions were observed in Preila and Rūgštelis

1 compared to Vilnius. The extreme average seasonal concentrations were between 0.8 and 1.3
2 $\mu\text{g m}^{-3}$ at Rūgšteliškis during fall and winter, between 0.9 and 1.1 $\mu\text{g m}^{-3}$ at Preila during
3 spring and winter, and between 0.4 and 0.6 $\mu\text{g m}^{-3}$ in Vilnius during summer and winter.
4 These values do not evidence clear seasonal trends, but highlight a site-to-site variability
5 which will be further discussed in the following. S-OOA instead was the largest contributor to
6 total OM during summer with an average concentration of $1.2 \pm 0.8 \mu\text{g m}^{-3}$, always agreeing
7 between sites within a confidence interval of 95% (2 tails t-test). By contrast, during winter
8 the S-OOA concentration dropped to an average value of $0.3 \pm 0.2 \mu\text{g m}^{-3}$, with 81% of the
9 points not statistically different from 0 $\mu\text{g m}^{-3}$ within 3σ . Finally, the LOA factor showed
10 statistically significant contributions within 3σ only during summer and late spring in Vilnius.
11 Despite its considerable day-to-day variability this factor contributed $1.0 \pm 0.8 \mu\text{g m}^{-3}_{\text{avg}}$ in
12 Vilnius during summer.

13 The markers source apportionment instead attributed $85\%_{\text{avg}}$ of the Other-OA_{marker} mass to the
14 SO_4^{2-} -related SOA, while NO_3^- -related SOA, MSA-related SOA, and PBOA explained
15 respectively $9\%_{\text{avg}}$, $5\%_{\text{avg}}$ and $1\%_{\text{avg}}$ of the Other-OA_{marker} mass (Fig. S13). The SO_4^{2-} -related
16 SOA average concentration was $2.4 \mu\text{g m}^{-3}$ during summer and $1.7 \mu\text{g m}^{-3}$ during winter with
17 no significant differences from station to station, suggesting a regional origin of the factor.
18 The NO_3^- -related SOA concentration was $0.4 \mu\text{g m}^{-3}_{\text{avg}}$ during winter, only $0.03_{\text{avg}} \mu\text{g m}^{-3}$,
19 during summer, corresponding to $10\%_{\text{avg}}$ and 1% of the OA, respectively. Moreover, the NO_3^-
20 -related SOA during winter showed the highest average concentrations in Vilnius with $0.5 \mu\text{g}$
21 m^{-3} and the lowest in Rūgšteliškis with $0.3 \mu\text{g m}^{-3}_{\text{avg}}$. The MSA-related SOA instead
22 manifested the highest concentrations during summer with an average of $0.12 \mu\text{g m}^{-3}_{\text{avg}}$.
23 Higher values were observed during summer at the rural coastal site of Preila where the
24 average concentration was $0.28 \mu\text{g m}^{-3}_{\text{avg}}$ corresponding to $10\%_{\text{avg}}$ of the OM. Finally, the
25 PBOA factor exhibited the largest seasonal concentrations during spring at the rural terrestrial
26 site of Rūgšteliškis with an average of $0.05 \mu\text{g m}^{-3}_{\text{avg}}$, while the summer average
27 concentration was $0.02 \mu\text{g m}^{-3}$ consistent with the low PBOA estimates reported in Bozzetti et
28 al. (2016) for the submicron fraction during summer.

29 Many previous studies reported a source apportionment of organic and inorganic markers
30 concentrations (Viana et al., 2008 and references therein). In these studies SO_4^{2-} , NO_3^- , and
31 NH_4^+ were typically used as tracers for secondary aerosol factors commonly associated with

1 regional background and long-range transport; here we compare the apportionment of the
2 SOA factors obtained from the marker source apportionment and the OOA factors separated
3 by the offline-AMS source apportionment. Moreover, contrasting the two source
4 apportionments may provide insight into the origin of the OOA factors retrieved from the
5 offline-AMS source apportionment, and into the origin of the SOA factors resolved by the
6 offline-AMS source apportionment. To our knowledge an explicit comparison has not yet
7 been reported in the literature.

8 Table 2 reports the correlations between the time series of the Other-OA_{marker} factors and the
9 Other-OA_{offline-AMS} factors (Figs. 6 and S13). These correlations are mostly driven by seasonal
10 trends as none of these sources shows clear spikes except for LOA during summer in Vilnius.
11 Using the correlations coefficients we can identify the mostly related factors from the two
12 source apportionments.

13 The SO₄²⁻-related SOA explained the largest fraction of the Other-OA_{marker} mass (85%_{avg}),
14 and it was the only Other-OA_{marker} factor always exceeding the individual concentrations of
15 B-OOA and S-OOA, indicating that the variability explained by the SO₄²⁻-related SOA in the
16 marker-source apportionment is explained by both OOA factors in the offline-AMS source
17 apportionment. Moreover, the SO₄²⁻-related SOA seasonality seems consistent with the sum
18 of S-OOA and B-OOA with higher concentrations in summer than in winter. This observation
19 suggests that the OOA factors resolved by offline-AMS are mostly of secondary origin and
20 the SO₄²⁻-related SOA, typically resolved by the markersource apportionment, explains the
21 largest fraction of the OOA factors apportioned by offline-AMS which includes both biogenic
22 SOA and aged background OA.

23 The NO₃⁻-related SOA and the PBOA factors were mostly related to B-OOA as they showed
24 higher correlations with B-OOA than with S-OOA. The B-OOA factor therefore may explain
25 a small fraction of primary sources (PBOA), which however represents only 0.6%_{avg} of the
26 total OA. In detail, the NO₃-related SOA correlation with B-OOA was poor ($R = 0.21$), but
27 the correlation with LOA and S-OOA was negative (Table 2), suggesting that the mass
28 attributed by the markers source apportionment to NO₃-related SOA was fully attributed to
29 the B-OOA factor in the offline-AMS source apportionment. This is also confirmed by the
30 fact that the sum of LOA and S-OOA concentrations during winter (when the NO₃-related
31 SOA substantially contributed) was much smaller than the NO₃⁻-related SOA concentration,
32 which therefore was attributed to B-OOA.

1 The MSA-related SOA showed the highest correlation with the S-OOA factor, as the two
2 sources exhibited the highest concentrations during summer, although the MSA-related SOA
3 preferentially contributed at the rural coastal site of Preila. While we already discussed the
4 probable secondary biogenic origin of S-OOA, the correlation with the MSA-related SOA
5 suggests that the S-OOA factor, especially at the rural coastal site of Preila, explains also a
6 large fraction of the marine biogenic SOA. The correlation between the two factors is
7 therefore not surprising as the precursor emissions (dimethyl sulfide, isoprene and terpenes)
8 are strongly related to the temperature leading to higher summer MSA-related SOA and S-
9 OOA concentrations. Assuming all the MSA-related SOA to be explained by the S-OOA
10 factor, we estimate a marine biogenic SOA contribution to S-OOA of 27%_{avg} during summer
11 at Preila, while this contribution is lower at the other stations (12%_{avg} in Rūgšteliškis during
12 summer, 7% in Vilnius during spring, no summer data for Vilnius Fig. S13). As already
13 mentioned, here we assume all the MSA-related SOA to be related to marine secondary
14 biogenic emissions, however other studies also report MSA from terrestrial biogenic
15 emissions (Jardine et al., 2015), moreover a certain fraction of the MSA-related SOA can also
16 be explained by the B-OOA factor. Overall these findings indicate that the terrestrial sources
17 dominate the S-OOA composition, nevertheless the marine SOA sources may represent a
18 non-negligible fraction, especially at the marine site.

19 Another advantage obtained in coupling the two source apportionment results is the
20 possibility to study the robustness of the factor analyses by evaluating the consistency of the
21 two approaches as we already discussed for the primary OA and Other-OA fractions. Figure
22 S14b displays the ratio between PMF modelled WSOC and measured WSOC for the offline-
23 AMS case. A clear bias between Vilnius and the rural sites, can be observed, with a WSOC
24 overestimate of ~5% in Preila and Rūgšteliškis. While this overestimate is negligible for the
25 WSOC mass, it might have significant consequences on single factor concentrations. By
26 contrast for the markers source apportionment (Fig. S14a) the OM residuals are more
27 homogeneous. As we show in Fig. S6, these residuals marginally affect the apportionment of
28 combustion sources, as suggested by the well comparing estimates of BBOA and TEOA using
29 the two methods. Therefore, these residuals are more likely affecting non-combustion sources
30 (LOA, S-OOA and B-OOA). For the common days, the S-OOA concentration is not
31 statistically different at the different stations during summer (confidence interval of 95%),
32 indicating that the residuals are more likely affecting LOA and B-OOA, which instead show
33 site-to-site differences. Now, the PMF WSOC residuals appear at all seasons, also during

periods without significant LOA contribution in Vilnius. Therefore, we conclude that B-OOA is the factor most significantly affected by the difference in the WSOC residuals. We could best assess the residual effects by comparing the B-OOA_{offline-AMS} with that estimated using the other technique that seem to yield more homogeneous residuals: B-OOA_{marker}. Here B-OOA_{marker} is estimated as Other-OA_{markers} - LOA - S-OOA. While B-OOA_{offline-AMS} shows site-to-site differences, B-OOA_{markers} did not show statistically different concentrations at all stations within a confidence interval of 95%. Based on these observations, we conclude that observed site-to-site differences in B-OOA concentrations are likely to be related to model uncertainties.

4.5 $f\text{CO}^+$ vs. $f\text{CO}_2^+$

Figure 7 displays the water-soluble $f\text{CO}^+$ vs. $f\text{CO}_2^+$ scatter plot. A certain correlation ($R=0.63$) is seen, with $f\text{CO}_2^+$ values being higher than $f\text{CO}^+$ ($\text{CO}_2^+:\text{CO}^+$: 1st quartile 1.50, median 1.75, 3rd quartile 2.01), whereas a 1:1 $\text{CO}_2^+:\text{CO}^+$ ratio is assumed in standard AMS/ACSM analyses (Aiken et al., 2008; Canagaratna et al., 2007). Comparing the measured $\text{CO}_2^+:\text{CO}^+$ values for the bulk WSOM and for pure gaseous CO_2 might provide insight into the origin of the CO^+ fragment in the AMS. The fragmentation of pure gaseous CO_2 returned a $\text{CO}_2^+:\text{CO}^+$ ratio of 8.21_{avg} which is significantly higher than our findings for the water-soluble bulk OA (1.75_{med}). Assuming thermal decarboxylation of organic acids as the only source of CO_2^+ does not explain the observed $\text{CO}_2^+:\text{CO}^+$ ratio of 1.75_{med} and another large source of CO^+ has to be assumed. Therefore, the carboxylic acid decarboxylation can be considered as a minor source of CO^+ .

Figure 7a and Fig. 8 show that not only does the water-soluble (WS) $\text{CO}_2^+:\text{CO}^+$ ratio systematically differ from 1, but it also varies throughout the year with higher $\text{CO}_2^+:\text{CO}^+$ values associated with warmer temperatures (Fig. 7c). The lower $\text{CO}_2^+:\text{CO}^+$ ratios in winter are primarily due to BB, as the WSBOA factor profile showed the lowest $\text{CO}_2^+:\text{CO}^+$ ratio (1.20_{avg}) among all the apportioned WS factors (2.00_{avg} for B-OOA, 2.70_{avg} for S-OOA, and 2.70_{avg} for LOA). We observed a seasonal variation of the $\text{CO}_2^+:\text{CO}^+$ ratio also for the water-soluble OOA (S-OOA + B-OOA) mass spectral fingerprint. The $\text{CO}_2^+:\text{CO}^+$ ratio was slightly lower for B-OOA than for S-OOA (2.00_{avg} for B-OOA, 2.70 for S-OOA). Nevertheless, given the low S-OOA relative contribution during winter (Fig. 3), we note that the total OOA showed a slightly lower $\text{CO}_2^+:\text{CO}^+$ ratio during winter than in summer (Fig. S15), indicating

that the OOA mass spectral fingerprint evolves over the year, possibly because of different precursor concentrations, and different photochemical activity.

Fig. 7a shows that most of the measured $\{f\text{CO}^+;f\text{CO}_2^+\}$ combinations lies within the triangle defined by the BBOA, S-OOA and B-OOA $\{f\text{CO}^+;f\text{CO}_2^+\}$ combinations. The LOA factor $\{f\text{CO}^+;f\text{CO}_2^+\}$ combination lies within the triangle as well, but is anyways a minor source and thus unlikely to contribute to the $\text{CO}_2^+:\text{CO}^+$ variability. We parameterized the CO^+ variability as a function of the CO_2^+ , and $\text{C}_2\text{H}_4\text{O}_2^+$ fragment variabilities using a multi-parameter fit according to Eq. (8). CO_2^+ and $\text{C}_2\text{H}_4\text{O}_2^+$ were chosen as B-OOA and BBOA tracers, respectively, with B-OOA and BBOA being the factors that explained the largest fraction of the $f\text{CO}^+$ variability (85% together).

$$\text{CO}^+_i = a \cdot \text{CO}_2^+_i + b \cdot \text{C}_2\text{H}_4\text{O}_2^+_i \quad (8)$$

Although this parameterization is derived from the WSOM fraction CO_2^+ , $\text{C}_2\text{H}_4\text{O}_2^+$, and CO^+ originate from the fragmentation of oxygenated, i.e. mostly water-soluble compounds. Accordingly, this parameterization might also well represent the total bulk OA (as the offline-AMS recoveries of these oxygenated fragments are relatively similar: $R_{\text{CO}_2^+}=0.74$, $R_{\text{C}_2\text{H}_4\text{O}_2^+}=0.61$, Daellenbach et al., 2016). Note that this parameterization may represent very well the variation of CO^+ in an environment impacted by BBOA and OOA, but should be used with caution when other sources (such as COA) may contribute to CO^+ , CO_2^+ and $\text{C}_2\text{H}_4\text{O}_2^+$. In order to check the applicability of this parameterization to a PMF output, we recommend monitoring the CO_2^+ and $\text{C}_2\text{H}_4\text{O}_2^+$ variability explained by the OOA and BBOA factors. In case a large part of the CO_2^+ and $\text{C}_2\text{H}_4\text{O}_2^+$ variability is explained by OOA and BBOA, the parameterization should return accurate CO^+ values. The coefficients a and b of Eq. (8) were determined as 0.52 and 1.39 respectively, while the average fit residuals were estimated to be equal to 10% (Fig. S16). In contrast, parameterizing CO^+ as proportional to CO_2^+ only (as done in the standard AMS analysis scheme with coefficients updated to the linear fit between CO^+ and CO_2^+ (1.75)) yielded 20%_{avg} residuals, indicating that such a univariate function describes the CO^+ variation less precisely.

An alternative parameterization is presented in the SI in which the contribution of moderately oxygenated species (such as S-OOA) to CO^+ was also considered by using $\text{C}_2\text{H}_3\text{O}^+$ as an independent variable. We show that the dependence of CO^+ on $\text{C}_2\text{H}_3\text{O}^+$ is statistically significant (Fig. 7c) as also suggested by the PMF results (S-OOA contributes 12% to the CO^+ variability). However, the parameter relating CO^+ to $\text{C}_2\text{H}_3\text{O}^+$ is negative, because the

1 $\text{CO}^+:\text{CO}_2^+$ and $\text{CO}^+:\text{C}_2\text{H}_4\text{O}_2^+$ ratios are lower in moderately oxygenated species compared to
2 species present in BBOA and B-OOA. While this parameterization captures the variability of
3 CO^+ across the seasons better compared to a 2-parameter fit for the present dataset, it may be
4 more prone to biases in other environments due to the known contributions of other factors to
5 $\text{C}_2\text{H}_3\text{O}^+$. For example, cooking-influenced organic aerosol (COA) often accounts for a
6 significant fraction of $\text{C}_2\text{H}_3\text{O}^+$. For ambient datasets we propose the use of CO_2^+ and $\text{C}_2\text{H}_4\text{O}_2^+$
7 only, which may capture less variation but is also less prone to biases. Although our results
8 suggest that the available CO^+ and O:C estimates (Aiken et al., 2008; Canagaratna et al.,
9 2015) may not well capture the CO^+ variability, our CO^+ parameterization should not be
10 applied to calculate the O:C ratios or recalculate the OA mass from AMS datasets, as those
11 are calibrated assuming a standard fragmentation table (i.e. $\text{CO}_2^+ = \text{CO}^+$).

12 In a recent work, Canagaratna et al. (2015) reported the Ar nebulization of water soluble
13 single compounds to study the HR-AMS mass spectral fingerprints in order to improve the
14 calculation of O:C and OM:OC ratios. Following the same procedure, we nebulized a subset
15 of the same standard compounds including malic acid, azelaic acid, citric acid, tartaric acid,
16 cis-pinonic acid, and D(+)-mannose. We obtained comparable $\text{CO}_2^+:\text{CO}^+$ ratios (within 10%)
17 to those of Canagaratna et al. (2015) for all the analyzed compounds, highlighting the
18 comparability of results across different instruments. With the exception of some
19 multifunctional compounds (citric acid, malic acid tartaric acid, ketobutyric acid, hydroxyl
20 methylglutaric acid, pyruvic acid, oxaloacetic acid, tartaric acid, oxalic acid and malonic
21 acid), the water-soluble single compounds analyzed by Canagaratna et al. (2015) mostly
22 showed $\text{CO}_2^+:\text{CO}^+$ ratios <1 , systematically lower than the $\text{CO}_2^+:\text{CO}^+$ ratios measured for the
23 bulk WSOM in Lithuania (1st quartile 1.50, median 1.75, 3rd quartile 2.01), which represents a
24 large fraction of the total OM (bulk EE: median = 0.59, 1st quartile = 0.51, 3rd quartile = 0.72).
25 Considering the relatively high bulk EE, and considering that the CO^+ and CO_2^+
26 fragmentation precursors tend to be more water soluble than the bulk OA, the aforementioned
27 compounds could be representative of a large part of the CO^+ and CO_2^+ fragmentation
28 precursors. This indicates that the selection of appropriate reference compounds for ambient
29 OA is non-trivial, and the investigation of multifunctional compounds is of high importance.

30

5 Conclusions

PM₁ filter samples were collected over an entire year (November 2013 to October 2014) at three different stations in Lithuania. Filters were analyzed by water extraction followed by nebulization of the liquid extracts and subsequent measurement of the generated aerosol with an HR-ToF-AMS (Daellenbach et al., 2016). For the first time, the nebulization step was conducted in Ar, enabling direct measurement of the CO⁺ ion, which is typically masked by N₂⁺ in ambient air and assumed to be equal to CO₂⁺ (Aiken et al., 2008). CO₂⁺:CO⁺ values >1 were systematically observed, with a mean ratio of 1.7±0.3. This is likely an upper limit for ambient aerosol, as only the water-soluble OM fraction is measured by the offline-AMS technique. CO⁺ concentrations were parameterized as a function of CO₂⁺, and C₂H₄O₂⁺, and this two-variable parameterization showed a superior performance to a parameterization based on CO₂⁺ alone, because CO⁺ and CO₂⁺ show different seasonal trends.

PMF analysis was conducted on both the offline-AMS data described above and a set of molecular markers together with total OM. Biomass burning was found to be the largest OM source in winter, while secondary OA was largest in summer. However, higher concentrations of primary anthropogenic sources (biomass burning and hopanes here used as traffic markers) were found at the urban background station of Vilnius. The offline-AMS and marker-based analyses also identified local emissions and primary biological particles, respectively, as factors with low overall but episodically important contributions to PM. Both methods showed traffic exhaust emissions to be only minor contributors to the total OM; which is not surprising given the distance of the three sampling stations from busy roads.

The two PMF analyses apportioned SOA to sources in different ways. The offline-AMS data yielded factors related to regional background (B-OOA) and temperature-driven (likely biogenic-influenced) emissions (S-OOA), while the marker-PMF yielded factors related to nitrate, sulfate, and MSA. For the offline-AMS PMF, S-OOA was the dominant factor in summer and showed a positive exponential correlation with the average daily temperature, similar to the behavior observed by Leaitch et al. (2011) in a Canadian boreal forest. Combining the two source apportionment techniques suggests that the S-OOA factor includes contributions from both terrestrial and marine secondary biogenic sources, while only small PBOA contributions to submicron OOA factors are possible. The analysis highlights the importance of regional meteorological conditions on air pollution in the southeastern Baltic region, as evidenced by simultaneous high BBOA levels at the three stations during three

different episodes in winter and by statistically similar S-OOA concentrations across the three stations during summer.

Acknowledgements

The research leading to these results received funding from the Lithuanian–Swiss Cooperation Programme “Research and Development” project AEROLIT (Nr. CH-3-ŠMM-01/08). JGS acknowledges the support of the Swiss National Science Foundation (Starting Grant No. BSSGI0 155846). IE-H acknowledges the support of the Swiss National Science Foundation (IZERZ0 142146).

1 References

- 2 Aiken, A. C., DeCarlo, P. F., Kroll, J. H., Worsnop, D. R., Huffman, J. A., Docherty, K. S.,
3 Ulbrich, I. M., Mohr, C., Kimmel, J. R., Sueper, D., Sun, Y., Zhang, Q., Trimborn, A.,
4 Northway, M., Ziemann, P. J., Canagaratna, M. R., Onasch, T. B., Alfarra, M. R., Prevot, A.
5 S. H., Dommen, J., Duplissy, J., Metzger, A., Baltensperger, U., and Jimenez J. L. O/C and
6 OM:OC ratios of primary, secondary, and ambient organic aerosols with high-resolution time-
7 of-flight aerosol mass spectrometry. *Environ. Sci. Technol.* 42, 4478-4485, 2008.
- 8 Aksoyoglu, S., Keller, J., Barmpadimos, I., Oderbolz, D., Lanz, V. A., Prévôt, A. S. H., and
9 Baltensperger U.: Aerosol modelling in Europe with a focus on Switzerland during summer
10 and winter episodes, *Atmos. Chem. Phys.*, 11, 7355–7373, 2011.
- 11 Aksoyoglu, S., Keller, J., Ciarelli, G., Prévôt, A. S. H., and Baltensperger, U.: A model study
12 on changes of European and Swiss particulate matter, ozone and nitrogen deposition between
13 1990 and 2020 due to the revised Gothenburg protocol, *Atmos. Chem. Phys.*, 14, 13081-
14 13095, doi:10.5194/acp-14-13081-2014, 2014.
- 15 Alfarra, M. R., Prévôt, A. S. H., Szidat, S., Sandradewi, J., Weimer, S., Lanz, V. A.,
16 Schreiber, D., Mohr, M., and Baltensperger, U.: Identification of the mass spectral signature
17 of organic aerosols from wood burning emissions, *Environ. Sci. Technol.*, 41, 5770–5777,
18 2007.
- 19 Allan, J. D., Delia, A. E., Coe, H., Bower, K. N., Alfarra, M. R., Jimenez, J. L., Middlebrook,
20 A. M., Drewnick, F., Onasch, T. B., and Canagaratna, M. R.: A generalized method for the
21 extraction of chemically resolved mass spectra from Aerodyne aerosol mass spectrometer
22 data, *J. Aerosol Sci.* 35 , 909-922, 2004.
- 23 Allan, J. D., Jimenez, J. L., Williams, P. I., Alfarra, M. R., Bower, K. N., Jayne, J. T., Coe,
24 H., and Worsnop, D. R.: Quantitative sampling using an Aerodyne aerosol mass spectrometer:
25 1. Techniques of data interpretation and error analysis, *J. Geophys. Res.-Atmos.*, 108, 4090,
26 2003.
- 27 Baklanov, A., Schlünzen, K., Suppan, P., Baldasano, J., Brunner, D., Aksoyoglu, S.,
28 Carmichael, G., Douros, J., Flemming, J., Forkel, R., Galmarini, S., Gauss, M., Grell, G.,
29 Hirtl, M., Joffre, S., Jorba, O., Kaas, E., Kaasik, M., Kallos, G., Kong, X., Korsholm, U.,
30 Kurganskiy, A., Kushta, J., Lohmann, U., Mahura, A., Manders-Groot, A., Maurizi, A.,
31 Moussiopoulos, N., Rao, S. T., Savage, N., Seigneur, C., Sokhi, R. S., Solazzo, E.,

1 Solomos, S., Sørensen, B., Tsegas, G., Vignati, E., Vogel, B., and Zhang, Y.: Online coupled
2 regional meteorology chemistry models in Europe: current status and prospects, *Atmos.*
3 *Chem. Phys.*, 14, 317-398, doi:10.5194/acp-14-317-2014, 2014.

4 Besombes, J.-L., Maître, A., Patissier, O., Marchand, N., Chevron, N., Stoklov, M., Masclet,
5 P.: Particulate PAHs observed in the surrounding of a municipal incinerator.
6 *Atmos. Environ.* 35, 6093–6104, 2001.

7 Birch, M. E. and Cary, R. A.: Elemental carbon-based method for monitoring occupational
8 exposures to particulate diesel exhaust, *Aerosol Sci. and Tech.*, 25, 221–241, 1996.

9 Bozzetti, C., Daellenbach, K., R., Hueglin, C., Fermo, P., Sciare, J., Kasper-Giebl, A., Mazar,
10 Y., Abbaszade, G., El Kazzi, M., Gonzalez, R., Shuster Meiseles, T., Flasch, M., Wolf, R.,
11 Křepelová, A., Canonaco, F., Schnelle-Kreis, J., Slowik, J. G., Zimmermann, R., Rudich, Y.,
12 Baltensperger, U., El Haddad, I., and Prévôt, A. S. H.: Size-Resolved Identification,
13 Characterization, and Quantification of Primary Biological Organic Aerosol at a European
14 Rural Site, *Environ. Sci. Technol.*, doi: 10.1021/acs.est.5b05960, 2016.

15 Bressi, M., Sciare, J., Gherzi, V., Mihalopoulos, N., Petit, J.-E., Nicolas, J. B., Moukhtar, S.,
16 Rosso, A., Féron, A., Bonnaire, N., Poulakis, E., and Theodosi, C.: Sources and geographical
17 origins of fine aerosols in Paris (France), *Atmos. Chem. Phys.*, 14, 8813–8839, 2014.

18 Brown, S. G., Eberly, S., Paatero, P., and Norris, G. A., Methods for estimating uncertainty in
19 PMF solutions: Examples with ambient air and water quality data and guidance on reporting
20 PMF results, *Sci. Tot. Environ.* 518-519, 626-635, 2015.

21 Bruns, E. A., Krapf, M., Orasche, J., Huang, Y., Zimmermann, R., Drinovec, L., Močnik, G.,
22 El-Haddad, I., Slowik, J. G., Dommen, J., Baltensperger, U. and Prévôt, A. S. H.:
23 Characterization of primary and secondary wood combustion products generated under
24 different burner loads, *Atmos. Chem. Phys.*, 15, 2825–2841, 2015.

25 Budisulistiorini, S. H., Canagaratna, M. R., Croteau, P. L., Marth, W. J., Baumann, K.,
26 Edgerton, E. S., Shaw, S. L., Knipping, E. M., Worsnop, D. R., Jayne, J. T., Gold, A., and
27 Surratt, J. D.: Real-Time Continuous Characterization of Secondary Organic Aerosol Derived
28 from Isoprene Epoxydiols in Downtown Atlanta, Georgia, Using the Aerodyne Aerosol
29 Chemical Speciation Monitor, *Environ Sci Technol*, 47, 5686-5694, Doi 10.1021/Es400023n,
30 2013.

1 Byčenkienė, S., Ulevicius, V., Plauškaitė, K., Bozzetti, C., Fröhlich, R., Mordas, G., Slowik,
2 J. G., El Haddad, I., Canonaco, F., and Prévôt A. S. H.: Source apportionment of the
3 carbonaceous aerosols during wintertime over urban environment, *in prep.*

4 Canagaratna, M. R., Jayne, J. T., Jimenez, J. L., Allan, J. D., Alfarra, M. R., Zhang, Q.,
5 Onasch, T. B., Drewnick, F., Coe, H., Middlebrook, A., Delia, A., Williams, L. R., Trimborn,
6 A. M., Northway, M. J., DeCarlo, P. F., Kolb, C. E., Davidovits, P. and Worsnop, D. R.:
7 Chemical and microphysical characterization of ambient aerosols with the Aerodyne aerosol
8 mass spectrometer, *Mass Spectrom. Rev.* 26:185-222, 2007.

9 Canagaratna, M. R., Jimenez, J. L., Kroll, J. H., Chen, Q., Kessler, S. H., Massoli, P.,
10 Hildebrandt Ruiz, L., Fortner, E., Williams, L. R., Wilson, K. R., Surratt, J. D.,
11 Donahue, N. M., Jayne, J. T., and Worsnop, D. R.: Elemental ratio measurements of organic
12 compounds using aerosol mass spectrometry: characterization, improved calibration, and
13 implications, *Atmos. Chem. Phys.*, 15, 253-272, doi:10.5194/acp-15-253-2015, 2015.

14 Canonaco, F., Crippa, M., Slowik, J. G., Baltensperger, U., and Prévôt, A. S. H.: SoFi, an
15 IGOR-based interface for the efficient use of the generalized multilinear engine (ME-2) for
16 the source apportionment: ME-2 application to aerosol mass spectrometer data, *Atmos. Meas.*
17 *Tech.*, 6, 3649-3661, 2013.

18 Canonaco, F., Slowik, J. G., Baltensperger, U., and Prévôt, A. S. H.: Seasonal differences in
19 oxygenated organic aerosol composition: implications for emissions sources and factor
20 analysis. *Atmos. Chem. Phys.* 15, 6993-7002, 2015.

21 Cavalli, F., Viana, M., Yttri, K. E., Genberg, J., and Putaud, J. P.: Toward a standardised
22 thermal-optical protocol for measuring atmospheric organic and elemental carbon: the
23 EUSAAR protocol, *Atmos. Meas. Tech.*, 3, 79-89, 2010.

24 Chow, J., Watson, J., Ashbaugh, L. L., and Magliano, K. L.: Similarities and differences in
25 PM₁₀ chemical source profiles for geological dust from the San Joaquin Valley, California.
26 *Atmos. Environ.* 37, 1317-1340, 2003.

27 Crippa, M., Canonaco, F., Lanz, V. A., Äijälä, M., Allan, J. D., Carbone, S., Capes, G.,
28 Ceburnis, D., Dall'Osto, M., Day, D. A., DeCarlo, P. F., Ehn, M., Eriksson, A., Freney, E.,
29 Hildebrandt Ruiz, L., Hillamo, R., Jimenez, J. L., Junninen, H., Kiendler-Scharr, A.,
30 Kortelainen, A. M., Kulmala, M., Laaksonen, A., Mensah, A. A., Mohr, C., Nemitz, E.,
31 O'Dowd, C., Ovadnevaite, J., Pandis, S. N., Petäjä, T., Poulain, L., Saarikoski, S., Sellegri, K.,

1 Swietlicki, E., Tiitta, P., Worsnop, D. R., Baltensperger, U., and Prévôt, A. S. H.: Organic
2 aerosol components derived from 25 AMS data sets across Europe using a consistent ME-2
3 based source apportionment approach, *Atmos. Chem. Phys.*, 14, 6159–6176, 2014.

4 Crippa, M., El Haddad, I., Slowik, J. G., DeCarlo, P.F., Mohr, C., Heringa, M. F., Chirico, R.,
5 Marchand, N., L., Sciare, J., Baltensperger, U., and Prévôt, A. S. H.: Identification of marine
6 and continental aerosol sources in Paris using high resolution aerosol mass spectrometry, *J.*
7 *Geophys. Res.*, 118, 1950-1963, 2013.

8 Daellenbach, K. R., Bozzetti, C., Krepeleva, A., Canonaco, F., Huang, R.-J., Wolf, R., Zotter,
9 P., Crippa, M., Slowik, J., Zhang, Y., Szidat, S., Baltensperger, U., Prévôt, A. S. H., and El
10 Haddad, I.: Characterization and source apportionment of organic aerosol using offline
11 aerosol mass spectrometry, *Atmos. Meas. Tech.*, 9, 23-39, 2016.

12 Davison, A. C. and Hinkley, D. V.: *Bootstrap Methods and Their Application*, Cambridge
13 University Press, Cambridge, UK, 582 pp., 1997.

14 DeCarlo, P. F., Kimmel, J. R., Trimborn, A., Northway, M. J., Jayne, J. T., Aiken, A. C.,
15 Gonin, M., Fuhrer, K., Horvath, T., Docherty, K. S., Worsnop, D. R., and Jimenez, J. L.:
16 Field-deployable, high-resolution, time-of-flight aerosol mass spectrometer, *Anal. Chem.*, 78,
17 8281–8289, 2006.

18 Dockery, D. W., Luttmann-Gibson, H., Rich, D. Q., Link, M. S., Mittleman, M. A., Gold, D.
19 R., Koutrakis, P., Schwartz, J. D., and Verrier, R. L.: Association of air pollution with
20 increased incidence of ventricular tachyarrhythmias recorded by implanted cardioverter
21 defibrillators, *Environ. Health Perspect.* 113:670-674, 2005.

22 Docherty, K. S., Aiken, A. C., Huffman, J. A., Ulbrich, I. M., DeCarlo, P. F., Sueper, D.,
23 Worsnop, D. R., Snyder, D. C., Peltier, R. E., Weber, R. J., Grover, B. D., Eatough, D. J.,
24 Williams, B. J., Goldstein, A. H., Ziemann, P. J., and Jimenez, J. L.: The 2005 Study of
25 Organic Aerosols at Riverside (SOAR-1): instrumental intercomparisons and fine particle
26 composition, *Atmos. Chem. Phys.*, 11, 12387-12420, doi:10.5194/acp-11-12387-2011, 2011.

27 Dudoitis, V., Byčenkienė, S., Plauškaitė, K., Bozzetti, C., Fröhlich, R., Mordas, G., and
28 Ulevicius V.: Spatial distribution of carbonaceous aerosol in the southeastern Baltic region
29 (event of grass fires), *Acta Geophys.*, 64, 711-731, 2016.

30 El Haddad, I., D'Anna, B., Temime-Roussel, B., Nicolas, M., Boreave, A., Favez, O., Voisin,
31 D., Sciare, J., George, C., Jaffrezo, J.-L., Wortham, H., and Marchand, N.: Towards a better

1 understanding of the origins, chemical composition and aging of oxygenated organic aerosols:
 2 case study of a Mediterranean industrialized environment, Marseille, *Atmos. Chem. Phys.*, 13,
 3 7875-7894, doi:10.5194/acp-13-7875-2013, 2013.

4 El Haddad, I., Marchand, N., Dron, J., Temime-Roussel, B., Quivet, E., Wortham, H.,
 5 Jaffrezo, J. L., Baduel, C., Voisin, D., Besombes, J. L., and Gille, G.: Comprehensive primary
 6 particulate organic characterization of vehicular exhaust emissions in France, *Atmos.*
 7 *Environ.*, 43, 6190–6198, 2009.

8 Elser, M., Bozzetti, C., El-Haddad, I., Maasikmets, M., Teinemaa, E., Richter, R., Wolf, R.,
 9 Slowik, J. G., Baltensperger, U., and Prévôt, A. S. H.: Urban increments of gaseous and
 10 aerosol pollutants and their sources using mobile aerosol mass spectrometry measurements,
 11 *Atmos. Chem. Phys. Discuss.*, doi:10.5194/acp-2016-31, 2016.

12 Elser, M., Huang, R.-J., Wolf, R., Slowik, J. G., Wang, Q., Canonaco, F., Li, G., Bozzetti, C.,
 13 Daellenbach, K. R., Huang, Y., Zhang, R., Li, Z., Cao, J., Baltensperger, U., El-Haddad, I.,
 14 and Prévôt, A. S. H.: New insights into PM_{2.5} chemical composition and sources in two
 15 major cities in China during extreme haze events using aerosol mass spectrometry, *Atmos.*
 16 *Chem. Phys.*, 16, 3207-3225, doi:10.5194/acp-16-3207-2016, 2016.

17 Fraser, M. P., Cass, G. R., and Simoneit, B. R. T.: Gas-phase and particle-phase organic
 18 compounds emitted from motor vehicle traffic in a Los Angeles roadway tunnel, *Environ. Sci.*
 19 *Technol.* 14, 2051-2060, 1998.

20 Fröhlich, R., Cubison, M. J., Slowik, J. G., Bukowiecki, N., Prevot, A. S. H., Baltensperger,
 21 U., Schneider, J., Kimmel, J. R., Gonin, M., Rohner, U., Worsnop, D. R. and Jayne J. T.: The
 22 ToF-ACSM: a portable aerosol chemical speciation monitor with TOFMS detection, *Atmos.*
 23 *Meas. Tech.*, 6, 3225-3241, 2013.

24 Golly, B., Brulfert, G., Berlioux G., Jaffrezo J.-L., Besombes, J.-L.: Large chemical
 25 characterisation of PM₁₀ emitted from graphite material production: Application in source
 26 apportionment, *Sci. Tot. Environ.*, 538, 634–643, 2015.

27 Guenther, A., Karl, T., Harley, P., Wiedinmyer, C., Palmer, P. I., and Geron, C.: Estimates of
 28 global terrestrial isoprene emissions using MEGAN (Model of Emissions of Gases and
 29 Aerosols from Nature), *Atmos. Chem. Phys.*, 6, 3181-3210, doi:10.5194/acp-6-3181-2006,
 30 2006.

1 He, L.-Y., Hu, M., Zhang, Y.-H., Huang, X.-F. and Yao, T.-T: Chemical characterization of
 2 fine particles from on-road vehicles in the Wutong tunnel in Shenzhen, China, *Chemosphere*
 3 62, 1565-1573, 2006.

4 He, L.-Y., Hu, M., Zhang, Y.-H., Huang, X.-F., and Yao, T.-T. Fine particle emissions from
 5 onroad vehicles in the Zhujiang tunnel, China, *Environ. Sci. Technol.*, 42, 4461-4466, 2008.

6 Herich, H., Gianini, M. F. D., Piot, C., Močnik, G., Jaffrezo, J. L., Besombes, J. L., Prévôt, A.
 7 S. H., and Hueglin, C.: Overview of the impact of wood burning emissions on carbonaceous
 8 aerosols and PM in large parts of the Alpine region, *Atmos. Environ.*, 89, 64–75,
 9 doi:10.1016/j.atmosenv.2014.02.008, 2014.

10 Hu, W. W., Campuzano-Jost, P., Palm, B. B., Day, D. A., Ortega, A. M., Hayes, P. L.,
 11 Krechmer, J. E., Chen, Q., Kuwata, M., Liu, Y. J., de Sá, S. S., McKinney, K., Martin, S. T.,
 12 Hu, M., Budisulistiorini, S. H., Riva, M., Surratt, J. D., St. Clair, J. M., Isaacman-Van Wertz,
 13 G., Yee, L. D., Goldstein, A. H., Carbone, S., Brito, J., Artaxo, P., de Gouw, J. A., Koss, A.,
 14 Wisthaler, A., Mikoviny, T., Karl, T., Kaser, L., Jud, W., Hansel, A., Docherty, K. S.,
 15 Alexander, M. L., Robinson, N. H., Coe, H., Allan, J. D., Canagaratna, M. R., Paulot, F., and
 16 Jimenez, J. L.: Characterization of a real-time tracer for isoprene epoxydiols-derived
 17 secondary organic aerosol (IEPOX-SOA) from aerosol mass spectrometer measurements,
 18 *Atmos. Chem. Phys.*, 15, 11807-11833, 10.5194/acp-15-11807-2015, 2015.

19 Huang, R.-J., Zhang, Y., Bozzetti, C., Ho, K.-F., Cao, J., Han, Y., Dällenbach, K. R., Slowik,
 20 J. G., Platt, S. M., Canonaco, F., Zotter, P., Wolf, R., Pieber, S. M., Bruns, E. A., Crippa, M.,
 21 Ciarelli, G., Piazzalunga, A., Schwikowski, M., Abbaszade, G., Schnelle-Kreis, J.,
 22 Zimmermann, R., An, Z., Szidat, S., Baltensperger, U., Haddad, I. E., and Prévôt, A. S. H.:
 23 High secondary aerosol contribution to particulate pollution during haze events in China,
 24 *Nature*, 514, 2014.

25 Jaffrezo, J.-L., Aymoz, G., Delaval, C., and Cozic J.: Seasonal evolution of the soluble
 26 fraction of particulate organic carbon in Alpine Valleys. *Atmos. Chem. Phys.*, 5, 2809-2821,
 27 2005.

28 Jaffrezo, J. L., Calas, T., and Bouchet, M.: Carboxylic acids measurements with ionic
 29 chromatography, *Atmos. Environ.*, 32, 2705–2708, 1998.

30 Jardine, K., Yañez-Serrano, A. M., Williams, J., Kunert, N., Jardine, A., Taylor, T., Abrell,
 31 L., Artaxo, P., Guenther, A., Hewitt, C. N., House, E., Florentino, A. P., Manzi, A., Higuchi,

1 N., Kesselmeier, J., Behrendt, T., Veres, P. R., Derstroff, B., Fuentes, J. D., Martin, S. T., and
 2 Andreae, M. O.: Dimethyl Sulfide in the Amazon Rain Forest, *Global Biogeochem. Cy.*, 29,
 3 19-32, 2015.

4 Klein, F., Platt, S. M., Farren, N. J., Detournay, A., Bruns, E. A., Bozzetti, C., Daellenbach,
 5 K. R., Kilic, D., Kumar, N. K., Pieber, S. M., Slowik, J. G., Temime-Roussel, B., Marchand,
 6 N., Hamilton, J. F., Baltensperger, U., Prévôt, A. S. H., and El Haddad, I.: Characterization of
 7 gas-phase organics using proton transfer reaction time-of-flight mass spectrometry: cooking
 8 emissions, *Environ. Sci. Technol.*, 50, 1243–1250, 2016.

9 Laden, F., Neas, L. M., Dockery, D. W., and Schwartz, J.: Association of fine particulate
 10 matter from different sources with daily mortality in six US cities, *Environ. Health Perspect.*
 11 108:941-947, 2000.

12 Lanz, V. A., Alfarra, M. R., Baltensperger, U., Buchmann, B., Hueglin, C., and Prévôt, A. S.
 13 H.: Source apportionment of submicron organic aerosols at an urban site by factor analytical
 14 modelling of aerosol mass spectra, *Atmos. Chem. Phys.*, 7, 1503-1522, doi:10.5194/acp-7-
 15 1503-2007, 2007.

16 Lanz, V. A., Prévôt, A. S. H., Alfarra, M. R., Weimer, S., Mohr, C., DeCarlo, P. F., Gianini,
 17 M. F. D., Hueglin, C., Schneider, J., Favez, O., D'Anna, B., George, C., and
 18 Baltensperger, U.: Characterization of aerosol chemical composition with aerosol mass
 19 spectrometry in Central Europe: an overview, *Atmos. Chem. Phys.*, 10, 10453–10471, 2010.

20 Leaitch, W. R. Macdonald, A. M., Brickell, P. C., Liggio, J., Sjostedt, S. J., Vlasenko, A.,
 21 Bottenheim, J. W., Huang, L., Li, S.-M., Liu, P. S. K., Toom-Sauntry, D., Hayden, K. A.,
 22 Sharma, S., Shantz, N. C., Wiebe H. A., Zhang, W., Abbatt, J. P. D., Slowik, J. G., Chang,
 23 Rachel, Y.-W., Russell, L. M., Schwartz, R. E., Takahama, S., Jayne, J. T., Ng, N. L.:
 24 Temperature response of the submicron organic aerosol from temperate forests, *Atmos.*
 25 *Environ.*, 45, 6696-6704, 2011.

26 Lee, A. K. Y., Herckes, P., Leaitch, W. R., Macdonald, A. M., and Abbatt, J. P. D.: Aqueous
 27 OH oxidation of ambient organic aerosol and cloud water organics: Formation of highly
 28 oxidized products, *Geoph. Res. Lett.*, 38, L11 805, 2011.

29 Li, S.M., Talbot, R.W., Barrie, L.A., Harriss, R.C., Davidson, C.I. and Jaffrezo, J.-L.:
 30 Seasonal and geographic variations of methanesulfonic acid in the Arctic troposphere, *Atmos.*
 31 *Environ.*, 27A, 3011-3024, 1993.

1 Lohmann, U., Broekhuizen, K., Leaitch, R., Shantz, N., and Abbatt, J.: How efficient is cloud
2 droplet formation of organic aerosols?, *Geophys. Res. Lett.* 31, L05108, 2004.

3 Manish K. S., Subramanian, R., Rogge, W. F., and Robinson, A. L.: Sources of organic
4 aerosol: Positive matrix factorization of molecular marker data and comparison of results
5 from different source apportionment models, *Atmos. Environ.*, 41, 9353-9369, 2007.

6 McMeeking, G. R., Bart, M., Chazette, P., Haywood, J. M., Hopkins, J. R., McQuaid, J. B.,
7 Morgan, W. T., Raut, J.-C., Ryder, C. L., Savage, N., Turnbull, K., and Coe, H.: Airborne
8 measurements of trace gases and aerosols over the London metropolitan region, *Atmos.*
9 *Chem. Phys.*, 12, 5163–5187, 2012.

10 Mihara, T. and Mochida, M.: Characterization of solvent-extractable organics in urban
11 aerosols based on mass spectrum analysis and hygroscopic growth measurement, *Envir. Sci.*
12 *Tech.*, 45, 9168–9174, 2011.

13 Mingui  n, M. C., Perron, N., Querol, X., Szidat, S., Fahrni, S. M., Alastuey, A., Jimenez, J.
14 L., Mohr, C., Ortega, A. M., Day, D. A., Lanz, V. A., Wacker, L., Reche, C., Cusack, M.,
15 Amato, F., Kiss, G., Hoffer, A., Decesari, S., Moretti, F., Hillamo, R., Teinila, K., Seco, R.,
16 Penuelas, J., Metzger, A., Schallhart, S., Muller, M., Hansel, A., Burkhardt, J. F.,
17 Baltensperger, U., and Prevot, A. S. H.: Fossil versus contemporary sources of fine elemental
18 and organic carbonaceous particulate matter during the DAURE campaign in Northeast Spain,
19 *Atmos. Chem. Phys.*, 11, 12067-12084, 2011.

20 Mohr, C., DeCarlo, P. F., Heringa, M. F., Chirico, R., Slowik, J. G., Richter, R., Reche, C.,
21 Alastuey, A., Querol, X., Seco, R., Penuelas, J., Jimenez, J. L., Crippa, M., Zimmermann, R.,
22 Baltensperger, U., and Prevot, A. S. H.: Identification and quantification of organic aerosol
23 from cooking and other sources in Barcelona using aerosol mass spectrometer data, *Atmos.*
24 *Chem. Phys.*, 12, 1649-1665, 2012.

25 Mordas, G., Plau  kait  , K., Prokop  ciuk, N., Dudoitis, V., Bozzetti, C. and Ulevicius, V.:
26 Observation of new particle formation on Curonian Spit located between continental Europe
27 and Scandinavia, *J Aerosol Sci*, 97, 38-55, 2016.

28 Ng, N. L., Herndon, S. C., Trimborn, A., Canagaratna, M. R., Croteau, P. L., Onasch, T. B.
29 Sueper, D., Worsnop, D. R., Zhang, Q., Sun, Y. L. and Jayne, J. T.: An Aerosol Chemical
30 Speciation Monitor (ACSM) for routine monitoring of the composition and mass
31 concentrations of ambient aerosol, *Aerosol Sci. Tech.*, 45, 770-784, 2011.

1 Paatero, P.: Least squares formulation of robust non-negative factor analysis, *Chemom. Intell.*
2 *Lab. Syst.*, 37, 23–35, 1997.

3 Paatero, P.: The multilinear engine - A table-driven, least squares program for solving
4 multilinear problems, including the n-way parallel factor analysis model, *J. Comput. Graph.*
5 *Stat.*, 8, 854-888, 1999.

6 Paatero, P. and Tapper, U.: Positive matrix factorization - a nonnegative factor model with
7 optimal utilization of error-estimates of data values, *Environmetrics*, 5, 111-126, 1994.

8 Rocke, D. M., and Lorenzato, S.: A two-component model for measurement error in
9 analytical chemistry, *Technometrics*, 37, 176-184, 1995.

10 Rutter, A. P., Snyder, D. C., Schauer, J. J., DeMinter, J. and Shelton, B.: Sensitivity and bias
11 of molecular marker-based aerosol source apportionment models to small contributions of
12 coal combustion soot, *Environ. Sci. Technol.*, 43, 7770-7777, 2009.

13 Schauer, J. J., Kleeman, M. J., Cass, G. R., and Simoneit, B. T.: Measurement of emissions
14 from air pollution sources. 3. C1-C29 organic compounds from fireplace combustion of
15 wood, *Environ. Sci. Technol.*, 35, 1716-1728, 2001.

16 Schwarze, P. E., Ovrevik, J., Lag, M., Refsnes, M., Nafstad, P., Hetland, R. B., and Dybing,
17 E.: Particulate matter properties and health effects: consistency of epidemiological and
18 toxicological studies, *Hum. Exp. Toxicol.* 25, 559-579, 2006.

19 Setyan, A., Zhang, Q., Merkel, M., Knighton, W. B., Sun, Y., Song, C., Shilling, J. E.,
20 Onasch, T. B., Herndon, S. C., Worsnop, D. R., Fast, J. D., Zaveri, R. A., Berg, L. K.,
21 Wiedensohler, A., Flowers, B. A., Dubey, M. K., and Subramanian R.: Characterization of
22 submicron particles influenced by mixed biogenic and anthropogenic emissions using high-
23 resolution aerosol mass spectrometry: results from CARES, *Atmos. Chem. Phys.*, 12, 8131-
24 8156, 2012.

25 Subramanian, R., Donahue, N. M., Bernardo-Bricker, A., Rogge, W. F., and Robinson, A. L.:
26 Contribution of motor vehicle emissions to organic carbon and fine particle mass in
27 Pittsburgh, Pennsylvania: Effects of varying source profiles and seasonal trends in ambient
28 marker concentrations, *Atmos. Environ.*, 40, 8002-8019, 2006.

29 Subramanian, R., Donahue, N. M., Bernardo-Bricker, A., Rogge, W. F., and Robinson, A. L.:
30 Insights into the primary-secondary and regional-local contributions to organic aerosol and
31 PM_{2.5} mass in Pittsburgh, Pennsylvania, *Atmos. Environ.*, 41, 7414-7433, 2007.

1 Sun, Y., Zhang, Q., Zheng, M., Ding, X., Edgerton, E. S., and Wang, X.: Characterization and
 2 source apportionment of water-soluble organic matter in atmospheric fine particles (PM_{2.5})
 3 with High-Resolution Aerosol Mass Spectrometry and GC-MS, *Envir. Sci. Tech.*, 45, 4854–
 4 4861, 2011.

5 Ulbrich, I. M., Canagaratna, M. R., Zhang, Q., Worsnop, D. R., and Jimenez, J. L.:
 6 Interpretation of organic components from positive matrix factorization of aerosol mass
 7 spectrometric data, *Atmos. Chem. Phys.*, 9, 2891-2918, 2009.

8 Ulevicius, V., Byčenkienė, S., Bozzetti, C., Vlachou, A., Plauškaitė, K., Mordas, G., Dudoitis,
 9 V., Abbaszade, G., Remeikis, V., Garbaras, A., Masalaite, A., Blees, J., Fröhlich, R.,
 10 Dällenbach, K. R., Canonaco, F., Slowik, J. G., Dommen, J., Zimmermann, R., Schnelle-
 11 Kreis, J., Salazar, G. A., Agrios, K., Szidat, S., El Haddad, I., and Prévôt, A. S. H.: Fossil and
 12 non-fossil source contributions to atmospheric carbonaceous aerosols during extreme spring
 13 grassland fires in Eastern Europe. *Atmos. Chem. Phys.*, 16, 5513-5529, 2016.

14 Viana, M., Kuhlbusch, T. A. J., Querol, X., Alastuey, A., Harrison, R. M., Hopke, P. K.,
 15 Winiwarter, W., Vallius, M., Szidat, S., Prévôt, A. S. H., Hueglin, C., Bloemen, H., Wählin,
 16 P., Vecchi, R., Miranda, A. I., Kasper-Giebl, A., Maenhaut, W., and Hitenberger, R.: Source
 17 apportionment of particulate matter in Europe: a review of methods and results, *J. Aerosol*
 18 *Sci.*, 39, 827–849, doi:10.1016/j.jaerosci.2008.05.007, 2008.

19 Waked, A., Favez, O., Alleman, L. Y., Piot, C., Petit, J. E., Delaunay, T., Golly, B.,
 20 Besombes, J.-L., Jaffrezo, J.-L., and Leoz-Garziandia, E.: Source apportionment of PM₁₀ in
 21 an urban site using a PMF model applied on inorganic and organic chemical species. *Atmos.*
 22 *Chem. Phys.*, 14, 3325-3346, 2014.

23 Xu, L., Guo, H., Boyd, C. M., Klein, M., Bougiatioti, A., Cerully, K. M., Hite, J. R.,
 24 Isaacman-VanWertz, G., Kreisberg, N. M., Knote, C., Olson, K., Koss, A., Goldstein, A. H.,
 25 Hering, S. V., de Gouw, J., Baumann, K., Lee, S.-H., Nenes, A., Weber, R. J., and Ng, N. L.:
 26 Effects of anthropogenic emissions on aerosol formation from isoprene and monoterpenes in
 27 the southeastern United States, *Proceedings of the National Academy of Sciences*, 112, 37-42,
 28 10.1073/pnas.1417609112, 2015.

29 Xu, L., Williams, L. R., Young, D. E., Allan, J. D., Coe, H., Massoli, P., Fortner, E., Chhabra,
 30 P., Herndon, S., Brooks, W. A., Jayne, J. T., Worsnop, D. R., Aiken, A. C., Liu, S.,
 31 Gorkowski, K., Dubey, M. K., Fleming, Z. L., Visser, S., Prévôt, A. S. H., and Ng, N. L.:

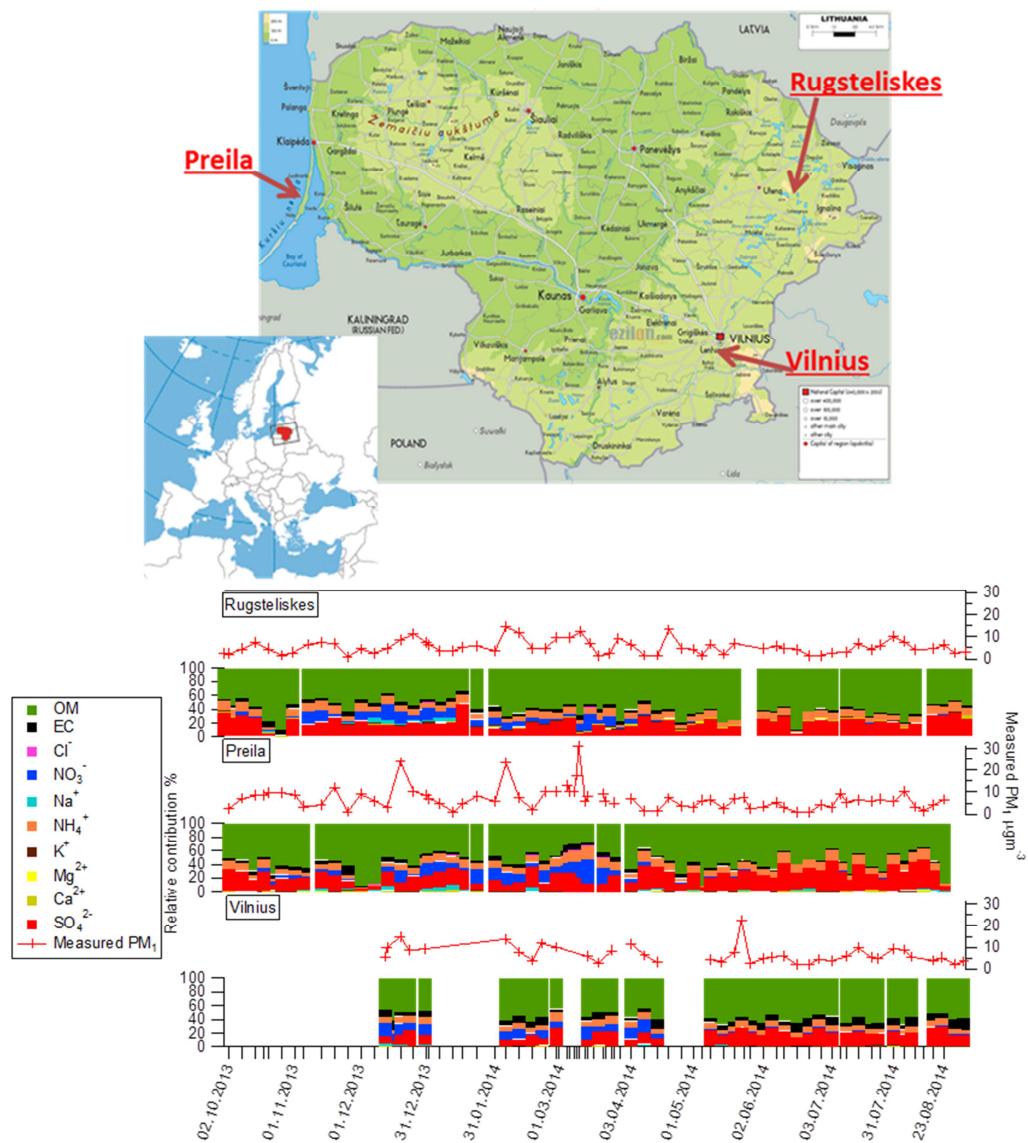
1 Wintertime aerosol chemical composition, volatility, and spatial variability in the greater
2 London area, *Atmos. Chem. Phys.*, 16, 1139-1160, 10.5194/acp-16-1139-2016, 2016.

3 Zhang, Q., Jimenez, J. L., Canagaratna, M. R., Ulbrich, I. M., Ng, N. L., Worsnop, D. R., and
4 Sun Y.: Understanding atmospheric organic aerosols via factor analysis of aerosol mass
5 spectrometry: a review. *Anal Bioanal. Chem.*, 401, 3045-3067, 2011.

6 Zotter, P., Ciobanu, V. G., Zhang, Y. L., El Haddad, I., Macchia, M., Daellenbach, K. R.,
7 Salazar, G. A., Huang, R.-J., Wacker, L., Hueglin, C., Piazzalunga, A., Fermo, P.,
8 Schwikowski, M., Baltensperger, U., Szidat, S., and Prévôt, A. S. H.: Radiocarbon analysis of
9 elemental and organic carbon in Switzerland during winter-smog episodes from 2008 to 2012
10 – Part 1: Source apportionment and spatial variability, *Atmos. Chem. Phys.*, 14, 13551–
11 13570, doi:10.5194/acp-14-13551-2014, 2014.

12

1 Figures main text



2

3 Figure 1. Sampling locations, and measured PM₁ composition. Ion concentrations from IC.

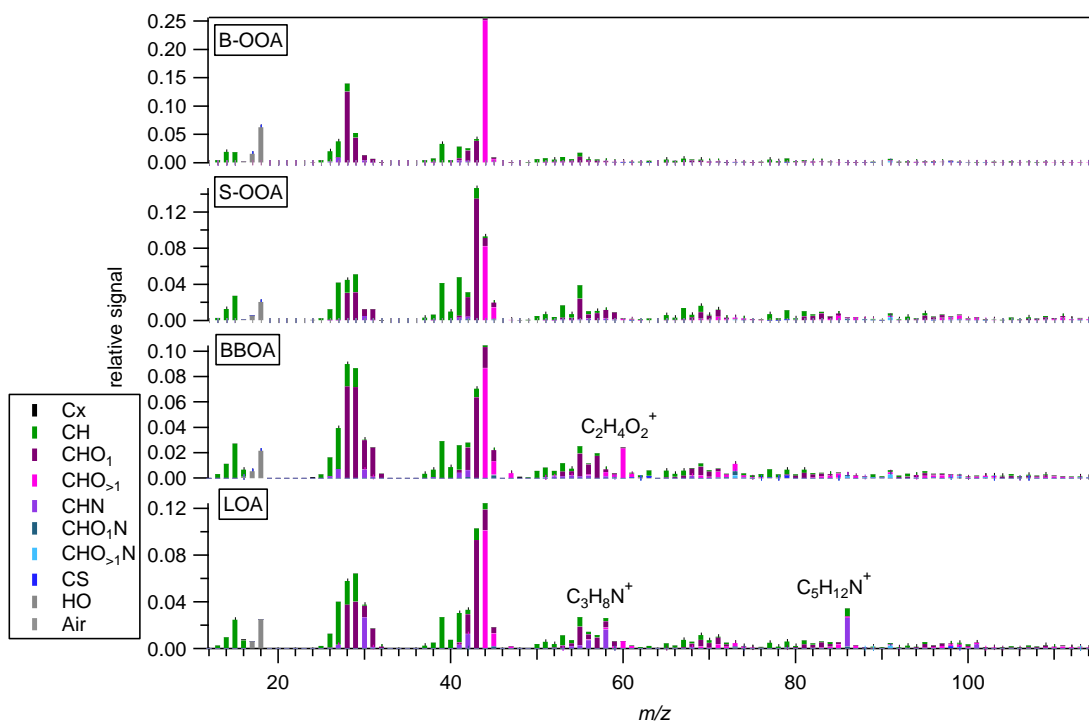


Figure 2. Offline-AMS PMF factor profiles: background oxygenated OA (B-OOA), summer oxygenated OA (S-OOA), biomass burning OA (BBOA), local OA (LOA).

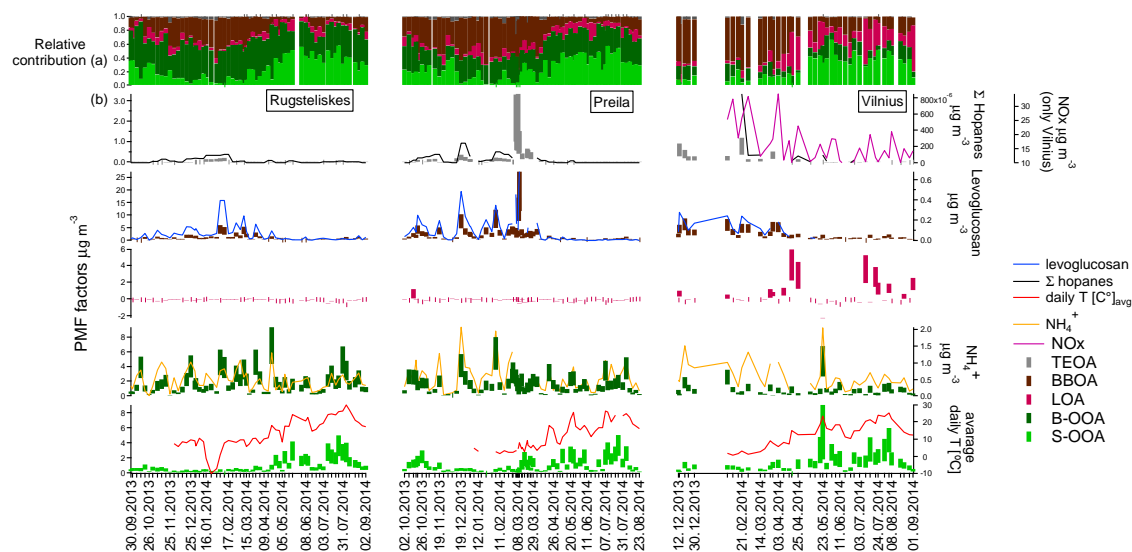
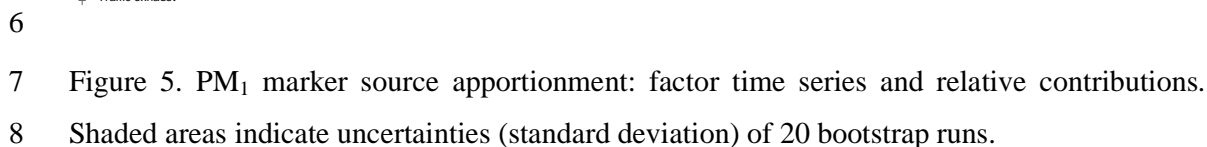
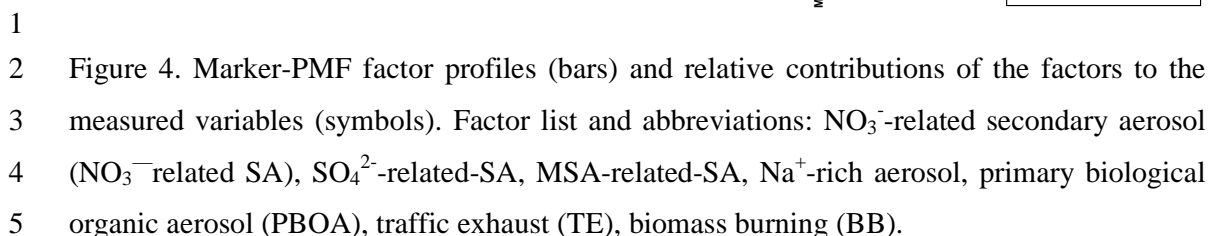


Figure 3. a) Temporal evolutions of relative contributions to the OA factors; b) OA sources and corresponding tracers: concentrations and uncertainties (shaded areas).



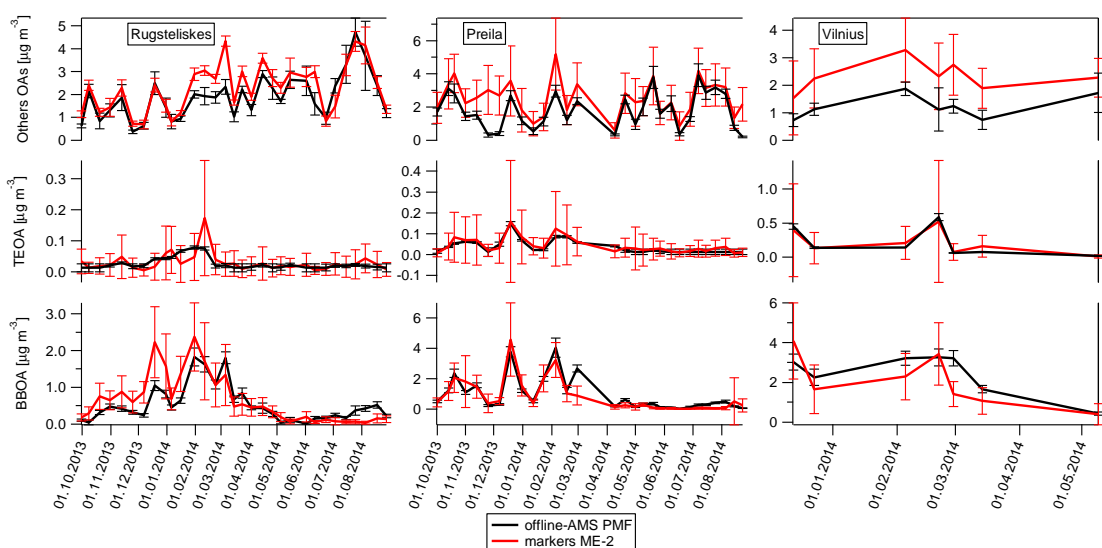


Figure 6. Marker-PMF and offline-AMS OM source apportionment comparison.

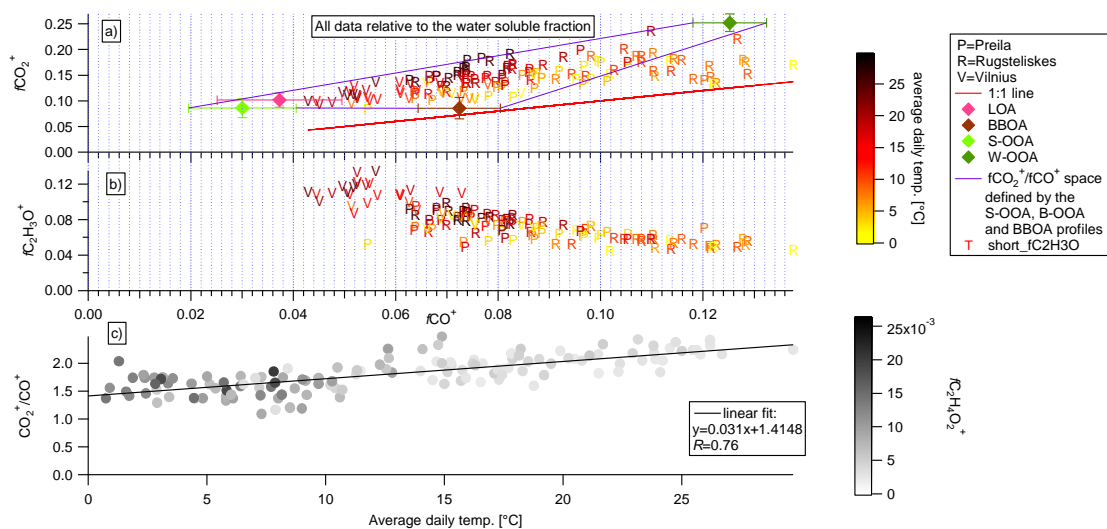
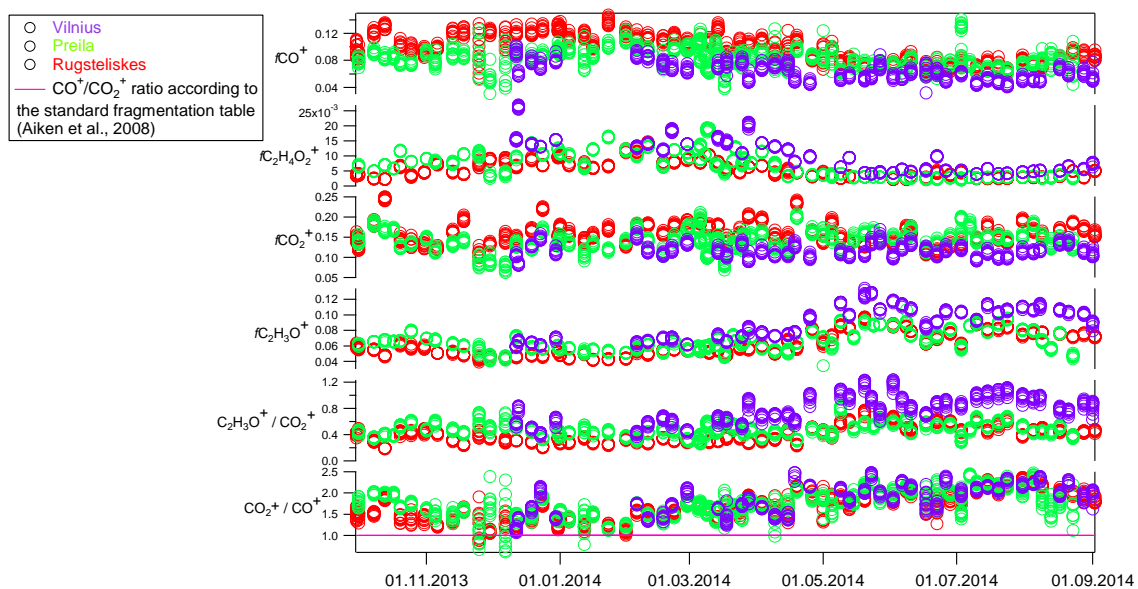


Figure 7. a) Water-soluble $f\text{CO}_2^+$ vs $f\text{CO}^+$ scatter plot. Color code denotes the average daily temperature [°C], diamonds indicate the $f\text{CO}_2^+;f\text{CO}^+$ ratio for different PMF factor profiles. The 1:1 line is displayed in red. Few points from Rūgšteliškis lie outside the triangle, suggesting they are not well explained by our PMF model. However, Fig. S5 displays flat residuals for Rūgšteliškis, indicating an overall good WSOM explained variability by the model. b) Water-soluble $f\text{C}_2\text{H}_3\text{O}^+$ vs $f\text{CO}^+$ scatter plot. Color code denotes the average daily temperature [°C] c) Scatter plot of the water-soluble CO_2^+ to CO^+ ratio vs. average daily temperature. Grey code denotes $f\text{C}_2\text{H}_4\text{O}_2^+$.



1

2 Figure 8. Time-dependent fractional contributions (f) of typical AMS tracers.

3